Alexandria Engineering Journal (2023) 76, 391–409

HOSTED BY

Alexandria University

Alexandria Engineering Journal

www.elsevier.com/locate/aej
www.sciencedirect.com

ORIGINAL ARTICLE

The new fractional discrete neural network model under electromagnetic radiation: Chaos, control and synchronization

Ahmed Salem Heilat [a], Rabia Chaimaà Karoun [b], Abdallah Al-Husban [c], Abderrahmane Abbes [d,*], Mohammed Al Horani [b], Giuseppe Grassi [e], Adel Ouannas [f]

[a] *Department of Mathematics, Faculty of Science and Information Technology, Jadara University, Irbid, Jordan*
[b] *Department of Mathematics, The University of Jordan, Amman 11942, Jordan*
[c] *Department of Mathematics, Faculty of Science and Technology, Irbid National University, P.O. Box: 2600, Irbid, Jordan*
[d] *Laboratory of Mathematics, Dynamics and Modelization, Badji Mokhtar-Annaba University, Annaba 23000, Algeria*
[e] *Dipartimento Ingegneria Innovazione, Universita del Salento, Lecce 73100, Italy*
[f] *Department of Mathematics and Computer Science, University of Larbi Ben M'hidi, Oum El Bouaghi 04000, Algeria*

Received 15 January 2023; revised 15 May 2023; accepted 6 June 2023
Available online 22 June 2023

KEYWORDS

Fractional discrete neural network model;
Incommensurate order;
Variable order;
Chaotic dynamics;
Control;
Synchronization

Abstract This paper describes a new four-dimensional fractional discrete neural network with electromagnetic radiation model. In addition, the non-linear dynamics of the suggested model are examined, within the framework of commensurate, incommensurate and variable orders, through different numerical techniques such as Lyapunov exponent, phase portraits, bifurcation diagrams, and the 0–1 test method. The results imply that The behaviours of the proposed fractional discrete neural network model have rich and complex dynamical properties that are influenced by the variation of the system parameters, the commensurate order, the incommensurate order and the variable order. Moreover, the approximate entropy test and C_o algorithm are carried out to measure complexity and validate the presence of chaos. Finally, nonlinear controllers are illustrated to stabilize and synchronize the proposed model.

1. Introduction

The neural networks is widely recognized as one of the most significant nonlinear models in the field of nonlinear studies. The structure and the capacity for parallel processing of these systems are the primary reasons for their significance. In recent years, neural networks (NN) theory has been receiving an increasing amount of attention from researchers owing to their various applications in many fields such as optimization, associative memory, data encryption, information processing and so on [1–5]. The dynamics of neural network model interactions have been widely investigated in the fields of mathematics and physics. The analyses study of these models found several rich dynamics, such as bifurcations, limit cycle, and chaotic

* Corresponding author.
E-mail address: abderrahmane.abbes@univ-annaba.dz (A. Abbes).
Peer review under responsibility of Faculty of Engineering, Alexandria University.

https://doi.org/10.1016/j.aej.2023.06.017
1110-0168

behaviors. Although numerous studies have explored the dynamic behaviors of continuous-time systems, discrete-time systems have received comparatively less attention. Discrete-time models possess their own distinct dynamical properties and a variety of practical problems can be represented through these systems in the real world. Owing to these characteristics, the study of discrete neural network systems is crucial and has led to significant advancements in engineering, physics, mathematics and other fields [6–9].

In the last two decades, discrete fractional calculus has caught the attention of numerous mathematicians intrigued by its applications in different domains such as hardware implementation, image encryption, and secure communication. Recently, a flurry of articles has been published on this hot issue, where the authors offer a variety of discrete-time fractional operators, stability analyses, and several theoretical results [10–14]. For instance, new mathematical modelling of human liver with Caputo–Fabrizio fractional derivative is studied in [15]. In [16], the authors present some applications of a regularized Ψ-Hilfer fractional derivative and the dynamics of the Fractional accelerated mass-spring system are analysed in [17]. The first study that concerns the modeling of the fractional chaotic map using the left Caputo difference operator and investigating its chaotic characteristics was introduced by Wu and Baleanu in [18]. These have led to the proposal of more commensurate fractional discrete chaotic systems, such as [19–21], and more incommensurate fractional discrete chaotic systems, such as [22–24], along with a variety of control strategies and synchronization schemes between different fractional chaotic maps, such as [25–27].

In recent times, a significant number of scholars have studied the dynamics of fractional continuous-time neural network models owing to their potential applications in different domains, like pattern recognition, combinatorial optimization, associative memory and signal processing [28–32]. Nonetheless, when continuous-time networks are implemented for computer-based computation, experimentation or simulation, it is essential to discretize continuous-time networks whenever they are used for computer-based calculation, experimentation, or simulation. Discrete-time neural networks (DTNNs) have been utilized in a diverse range of applications [33,34]. The discretization of the continuous-time counterpart does not sustain its dynamics (see [35]). Therefore, an investigation into the dynamics of DTNN is imperative. Recently, some research papers have appeared that examine the dynamical behaviour of fractional discrete-time neural network models [36–38]. For instance, the stability of fractional discrete-time neural networks models have been studied by Hioual et al. in [39]. The chaotic behaviour of a 3D fractional discrete Hopfield neural networks model has been analyzed by Abbes et al. [40]. In [41], the authors have explored the chaos and complexity of the incommensurate fractional discrete NN, while Almatroud in [42] discussed the extreme multistability of fractional discrete Hopfield neural networks model. The majority of the aforementioned discrete neural networks research are models with commensurate or incommensurate fractional orders, but unfortunately, as far as we know, very few research contributions have been performed to study the dynamic behaviors of fractional-order discrete-time neural network models with variable fractional orders [43–46]. Consequently, the investigation of the chaotic dynamics of neural network models based on fractional differences with commensurate, incommensurate and variable order, as well as their synchronization and control, is an attractive subject.

Motivated by the aforementioned discussion, we intend in this paper to explore and study the dynamic behaviors of the new four-dimensional fractional discrete neural network model with electromagnetic radiation using commensurate, incommensurate and variable orders. The basic properties of this fractional model will be studied using certain theoretical and numerical analyses. Furthermore, we will use the approximate entropy test and C_0 algorithm to measure the complexity and validate the presence of chaos in the proposed system. In addition, we propose nonlinear controllers that enable stabilizing and synchronizing the suggested model by forcing the states to converge toward zero asymptotically. Finally, we will conclude the study by summarizing the most significant findings obtained in the article.

The remainder of this paper is organized as follows. In Section 2, we provide the mathematical formulation of the fractional discrete neural network model with electromagnetic radiation using the Caputo difference operator. in Section 3, we explore the basic dynamical properties of the system through numerical and theoretical analyses. In Section 4, we employ the 0–1 method, the approximate entropy test ($ApEn$) and the C_0 algorithm to measure complexity and confirm the existence of chaos within the suggested model. In Section 5, we suggest adaptive controllers in order to stabilize and synchronize the chaotic trajectories of the proposed fractional discrete neural network model. Finally, the conclusion of the whole paper is presented in Section 6.

2. Model description of the fractional discrete Neural Network

Allehiany et al. [47] introduce a new neural network with electromagnetic radiation using Caputo fractional derivative ${}^{c}D^{q}$. In our work, we replace the Caputo derivative by the difference operator ${}^{c}\Delta_{d}^{\vartheta}$ to produce a novel fractional discrete neural network (FDNN) with electromagnetic radiation. The formulation of the mathematical form of the fractional DHH model is as follows:

$$\begin{cases} {}^{c}\Delta_{d}^{\vartheta} z_1(r) = -z_1(r-1+\vartheta) + a_1 \tanh(z_1(r-1+\vartheta)) + a_2 \tanh(z_2(r-1+\vartheta)) \\ \qquad\qquad +a_3 \tanh(z_3(r-1+\vartheta)), \\ {}^{c}\Delta_{d}^{\vartheta} z_2(r) = -z_2(r-1+\vartheta) + b_1 \tanh(z_1(r-1+\vartheta)) + b_2 \tanh(z_2(r-1+\vartheta)) \\ \qquad\qquad +b_3 \tanh(z_3(r-1+\vartheta)) + \alpha z_2(r-1+\vartheta)\left(e+\beta(z_4(r-1+\vartheta))^4\right), \\ {}^{c}\Delta_{d}^{\vartheta} z_3(r) = -z_3(r-1+\vartheta) + c_1 \tanh(z_1(r-1+\vartheta)) + c_2 \tanh(z_2(r-1+\vartheta)) \\ \qquad\qquad +c_3 \tanh(z_3(r-1+\vartheta)), \\ {}^{c}\Delta_{d}^{\vartheta} z_4(r) = d_1 z_2(r-1+\vartheta) + d_2 z_4(r-1+\vartheta), \end{cases} \tag{1}$$

where a_i, b_i, c_i $(i = 1, 2, 3), d_1, d_2, \alpha, \beta$ and e are real parameters. We take $0 < \vartheta \leqslant 1, r \in \mathbb{N}_{d+1-\vartheta}, N_d = \{d, d+1, d+2, \ldots\}$ such that $d \in \mathbb{R}$. ${}^{C}\Delta_{d}^{\vartheta}$ is the Caputo-like difference operator which is defined, according to [12], as

$${}^{C}\Delta_{d}^{\vartheta}\chi(r) = \Delta_{d}^{-(k-\vartheta)}\Delta^{k}\chi(r) = \frac{1}{\Gamma(k-\vartheta)}\sum_{v=k}^{r-(k-\vartheta)}(r-v-1)^{(k-1-\vartheta)}\Delta^{k}\chi(v), \tag{2}$$

where $r \in (\mathbb{N})_{d+k-\vartheta}$ and $k = \lceil \vartheta \rceil + 1$. $\Delta_{d}^{-\vartheta}$ is the $\vartheta - th$ fractional sum which, according to [10], can be given by

$$\Delta_{d}^{-\vartheta}\chi(r) = \frac{1}{\Gamma(\vartheta)}\sum_{v=\vartheta}^{r-\vartheta}(r-v-1)^{(\vartheta-1)}\chi(v), \quad r \in (\mathbb{N})_{k+\vartheta},\ \vartheta > 0. \tag{3}$$

In order to discuss the complex dynamics of system (1), we shall present the Lemma below, which will enable us to acquire the numerical formula for the discrete fractional predator–prey system:

Lemma 1. [18]The solution of the initial value problem **IVP**

$$\begin{cases} {}^{C}\Delta_{d}^{\vartheta}\chi(r) = g(r-1+\vartheta, \chi(r-1+\vartheta)) \\ \Delta^{k}\chi(d) = \chi_{j}, \quad n = [\vartheta]+1, \quad j = 0,1,\ldots,n-1, \end{cases} \tag{4}$$

is written as

$$\chi(r) = \chi_0(d) + \frac{1}{\Gamma(\vartheta)} \sum_{v=d+n-\vartheta}^{r-\vartheta} (r-1-v)^{(\vartheta-1)} g(v-1+\vartheta, \chi(v-1+\vartheta)), \quad r \in \mathbb{N}_{d+n}, \tag{5}$$

where

$$\chi_0(d) = \sum_{j=0}^{n-1} \frac{(r-d)^j}{\Gamma(k+1)} \Delta^j \chi(d). \tag{6}$$

Remark 1. Take $d = 0$, since $(r-1-v)^{(\vartheta-1)} = \frac{\Gamma(r-v)}{\Gamma(r+1-v-\vartheta)}$ and for $k = v+\vartheta-1$ and $n = 1$, the numerical formula (5) can be designed for $\vartheta \in (0,1]$ as follows:

$$\chi(r) = \chi(0) + \frac{1}{\Gamma(\vartheta)} \sum_{k=0}^{r-1} \frac{\Gamma(r-1-k+\vartheta)}{\Gamma(r-k)} \; g(k, \chi(k)). \tag{7}$$

3. Nonlinear dynamics of the FDNN model

In this part, the dynamics of the fractional discrete neural network model with electromagnetic radiation (1) will be examined in three cases: the commensurate order case, the incommensurate order case and the variable order case. These examinations will be conducted using different numerical analysis methods, such as display phase portraits, bifurcation diagrams, and maximum Lyapunov exponent (λ_{max}) estimations. The maximum Lyapunov exponents of the attractors of the fractional DNN model (1) will be calculated by using the Jacobian matrix method [48].

3.1. Commensurate order FDNN model

In this part, we will investigate the dynamics of the commensurate fractional discrete neural network model (1) We will discuss the characteristic of the proposed commensurate FDNN system (1). It should be noted that the system with commensurate order is a system of equations generated with identical orders. In light of this, we will now provide the numerical formula, which is derived from Lemma 1, as follows:

$$\begin{cases} z_1(r+1) = z_1(0) + \sum_{k=0}^{n} \frac{\Gamma(r-1-k+\vartheta)}{\Gamma(\vartheta)\Gamma(r-k)} (-z_1(k) + a_1 \tanh(z_1(k)) + a_2 \tanh(z_2(k)) \\ \qquad +a_3 \tanh(z_3(k))), \\ z_2(r+1) = z_2(0) + \sum_{k=0}^{n} \frac{\Gamma(r-1-k+\vartheta)}{\Gamma(\vartheta)\Gamma(r-k)} (-z_2(k) + b_1 \tanh(z_1(k)) + b_2 \tanh(z_2(k)) \\ \qquad +b_3 \tanh(z_3(k)) + \alpha z_2(k)\left(e + \beta(z_4(k))^4\right)\Big), \\ z_3(r+1) = z_3(0) + \sum_{j=0}^{n} \frac{\Gamma(r-1-k+\vartheta)}{\Gamma(\vartheta)\Gamma(r-k)} (-z_3(k) + c_1 \tanh(z_1(k)) + c_2 \tanh(z_2(k)) \\ \qquad +c_3 \tanh(z_3(k))), \\ z_4(r+1) = z_4(0) + \sum_{j=0}^{n} \frac{\Gamma(r-1-k+\vartheta)}{\Gamma(\vartheta)\Gamma(r-k)} (d_1 z_2(k) + d_2 z_4(k)), \quad r = 1,2,\cdots, \end{cases} \tag{8}$$

where $z_1(0), z_2(0), z_3(0)$ and $z_4(0)$ are the initial conditions. Setting the parameters system $a_1 = 1.5, a_2 = 2, a_3 = 0.9, b_1 = -1.5, b_2 = 1.5, b_3 = -0.45, c_1 = 3, c_2 = -2, c_3 = 1.5, d_1 = 0.1, d_2 = -0.45, \alpha = -0.5, \beta = -0.12, e = 1.519$ and the initial condition (I.C) $(z_1(0), z_2(0), z_3(0), z_4(0)) = (0, 0, 5.5, 5.5)$, the variation in the dynamic behaviour of the proposed system is illustrated with the help of bifurcation diagrams. The commensurate fractional order ϑ is regarded as the bifurcation parameter. Figs. 1a and 1b depict the bifurcation and the maximum Lyapunov exponents (λ_{max}) where the parameter system $e = 1.519$, while Figs. 1c and 1d show the bifurcation and t λ_{max} where $e = 1.65$. We can see that upon changing the commensurate order ϑ, the FDNN model (1) exhibits extremely complex dynamics involving chaos and periodic motion. In particular, when ϑ takes larger values, λ_{max} is negative or equal to zero, meaning that the commensurate FDNN (1) is stable and periodic windows appear. Moreover, when the commensurate order decreases, chaotic behaviors can be obtained where the values of λ_{max} are positive. If ϑ continues to decrease, the values of λ_{max} approaches zero, and the proposed commensurate FDNN model becomes periodic. We can also observe that when we change the value of the system parameter e from 1.519 to 1.65, the chaotic region expands and the commensurate fractional discrete neural network with electromagnetic radiation model (1) gets more chaotic. Now, considering e as the critical parameter, we plotted the bifurcation diagrams of (1) versus $e \in [1.35, 1.7]$ as shown in Fig. 2, which correspond to the fractional values $\vartheta = 0.56$, $\vartheta = 0.63$, $\vartheta = 0.75$ and $\vartheta = 0.99$. We notice that the states of the FDNN are affected by the system parameter e and the commensurate fractional order ϑ. For instance, when the orderϑ increases, the chaotic region shrinks and more periodic states are observed. Also, Figs. 2c and 2d show that when the system parameter e increases, the trajectories of the commensurate model (1) gradually evolve from a periodic state with an eight-period orbit to a chaotic one, and λ_{max} plotted in Figs. 2g and 2h confirm these findings. For completeness, to have a better understanding of these characteristics, Fig. 3 depicts the discrete time evolution of the states z_1, z_2, z_3 and z_4 of the proposed commensurate system (1) while Fig. 4 depicts the results of different phase portraits for $\gamma = 0.67$, $\gamma = 0.7$, $\gamma = 0.8$, $\gamma = 0.85$, $\gamma = 0.9$ and $\gamma = 0.95$ in 3D space. It is clear that the proposed commensurate fractional discrete system exhibits chaotic motion when the order ϑ decreases and periodic orbits when the commensurate order ϑ takes higher values. These numerical simulations demonstrate that the commensurate FDNN system (1) has various interesting dynamical properties.

3.2. Incommensurate order FDNN model

This section explores the behavior of the discrete neural network model with incommensurate fractional order values. The Incommensurate order system refers to the idea of using distinct fractional orders for each equation of the system. The incommensurate fractional discrete neural network model is represented as

$$\begin{cases} {}^{c}\Delta_{d}^{\vartheta_1} z_1(r) = -z_1(r-1+\vartheta_1) + a_1 \tanh(z_1(r-1+\vartheta_1)) + a_2 \tanh(z_2(r-1+\vartheta_1)) \\ \qquad +a_3 \tanh(z_3(r-1+\vartheta_1)), \quad r \in \mathbb{N}_{d-\vartheta_1+1} \\ {}^{c}\Delta_{d}^{\vartheta_2} z_2(r) = -z_2(r-1+\vartheta_2) + b_1 \tanh(z_1(r-1+\vartheta_2)) + b_2 \tanh(z_2(r-1+\vartheta_2)) \\ \qquad +b_3 \tanh(z_3(r-1+\vartheta_2)) + \alpha z_2(r-1+\vartheta_2) \\ \qquad \times\left(e + \beta(z_4(r-1+\vartheta_2))^4\right), \quad r \in \mathbb{N}_{d-\vartheta_2+1} \\ {}^{c}\Delta_{d}^{\vartheta_3} z_3(r) = -z_3(r-1+\vartheta_3) + c_1 \tanh(z_1(r-1+\vartheta_3)) + c_2 \tanh(z_2(r-1+\vartheta_3)) \\ \qquad +c_3 \tanh(z_3(r-1+\vartheta_3)), \quad r \in \mathbb{N}_{d-\vartheta_3+1} \\ {}^{c}\Delta_{d}^{\vartheta_4} z_4(r) = d_1 z_2(r-1+\vartheta_4) + d_2 z_4(r-1+\vartheta_4), \quad r \in \mathbb{N}_{d-\vartheta_4+1}. \end{cases} \tag{9}$$

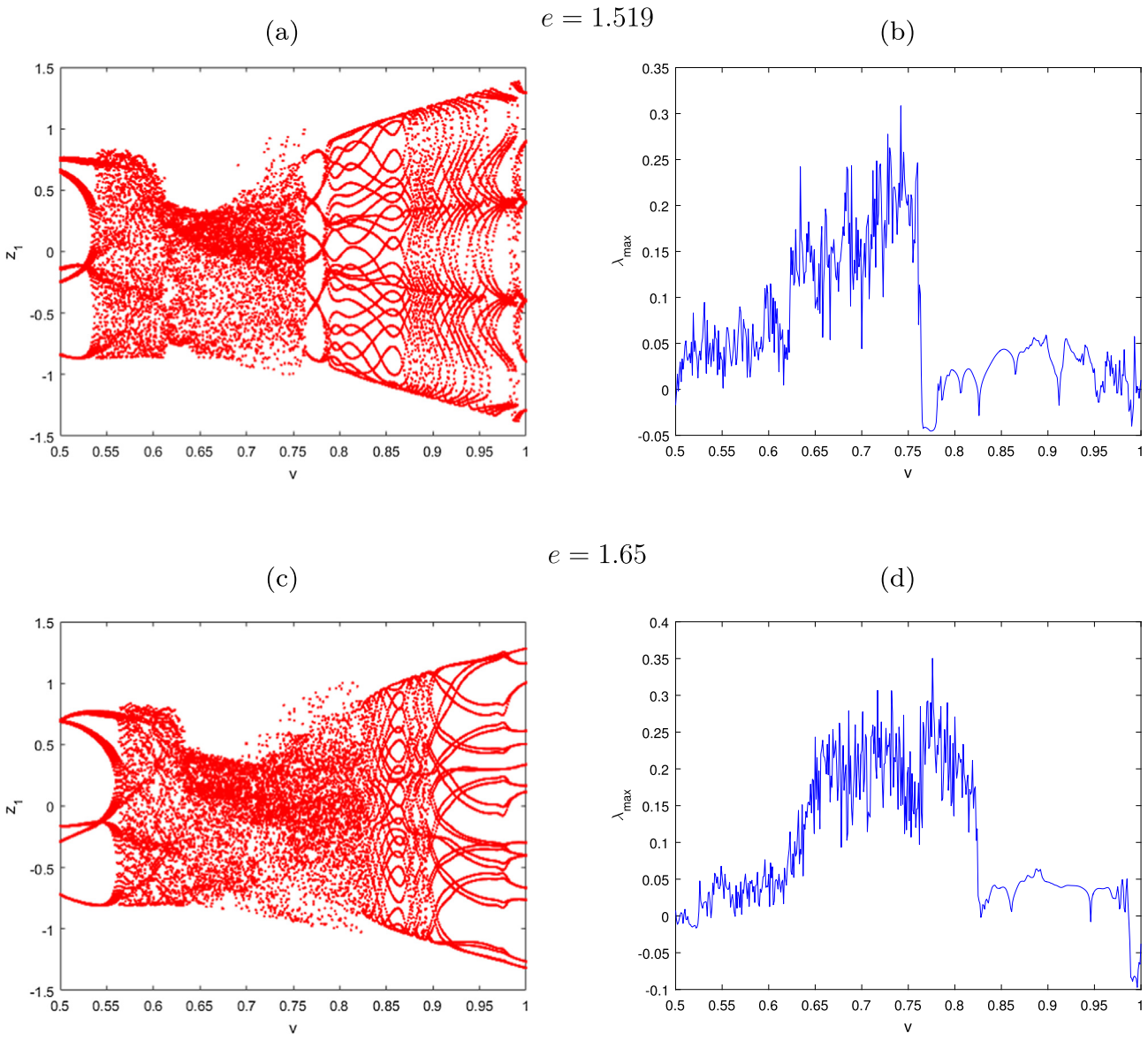

Fig. 1 The bifurcations and maximum Lyapunov exponents versus the fractional order ϑ of the commensurate FDNN (1).

Employing Lemma 1, the numerical model of the incommensurate fractional discrete system (9) is signed as follows:

$$\begin{cases} z_1(r+1) = z_1(0) + \sum_{k=0}^{n} \frac{\Gamma(r-1-k+\vartheta_1)}{\Gamma(\vartheta_1)\Gamma(r-k)}(-z_1(k) + a_1 \tanh(z_1(k)) + a_2 \tanh(z_2(k)) \\ \qquad +a_3 \tanh(z_3(k))), \\ z_2(r+1) = z_2(0) + \sum_{k=0}^{n} \frac{\Gamma(r-1-k+\vartheta_2)}{\Gamma(\vartheta_2)\Gamma(r-k)}(-z_2(k) + b_1 \tanh(z_1(k)) + b_2 \tanh(z_2(k)) \\ \qquad +b_3 \tanh(z_3(k)) + \alpha z_2(k)\left(e + \beta(z_4(k))^4\right)\Big), \\ z_3(r+1) = z_3(0) + \sum_{j=0}^{n} \frac{\Gamma(r-1-k+\vartheta_3)}{\Gamma(\vartheta_3)\Gamma(r-k)}(-z_3(k) + c_1 \tanh(z_1(k)) + c_2 \tanh(z_2(k)) \\ \qquad +c_3 \tanh(z_3(k))), \\ z_4(r+1) = z_4(0) + \sum_{j=0}^{n} \frac{\Gamma(r-1-k+\vartheta_4)}{\Gamma(\vartheta_4)\Gamma(r-k)}(d_1 z_2(k) + d_2 z_4(k)), \quad r = 1, 2, \cdots. \end{cases} \tag{10}$$

The three bifurcation diagrams in Fig. 5 reflect the behaviors of the incommensurate model by varying $e \in [1.35, 1.7]$ with the values of parameters $a_1 = 1.5, a_2 = 2, a_3 = 0.9, b_1 = -1.5, b_2 = 1.5, b_3 = -0.45, c_1 = 3, \ c_2 = -2, c_3 = 1.5, d_1 = \ 0.1, \ d_2 = -0.45, \alpha = -0.5, \beta = -0.12$ and the I.C $(0, 0, 5.5, 5.5)$. It is plain to observe that these diagrams are strictly different, indicating that the change in orders $(\vartheta_1, \vartheta_2, \vartheta_3, \vartheta_4)$ has an influence on the states of the incommensurate fractional discrete neural network model (9). For instance, for $(\vartheta_1, \vartheta_2, \vartheta_3, \vartheta_4) = (0.9, 1, 1, 0.9)$, we can observe that the system states evolve from chaotic to periodic when the parameter e increases. For $(\vartheta_1, \vartheta_2, \vartheta_3, \vartheta_4) = (0.9, 0.3, 1, 0.9)$, a chaotic region is observed throughout the interval except for a small region when e approaches 1.35, while for $(\vartheta_1, \vartheta_2, \vartheta_3, \vartheta_4) = (0.5, 1, 0.7, 1)$, when the parameter e increases abd close to 1.7, the incommensurate FDNN model (9) shows periodic regions with five-period orbits. Furthermore, we investigate the following three cases for a more accurate illustration of the influence of incommensurate orders on the behaviours of the FDNN model (9):

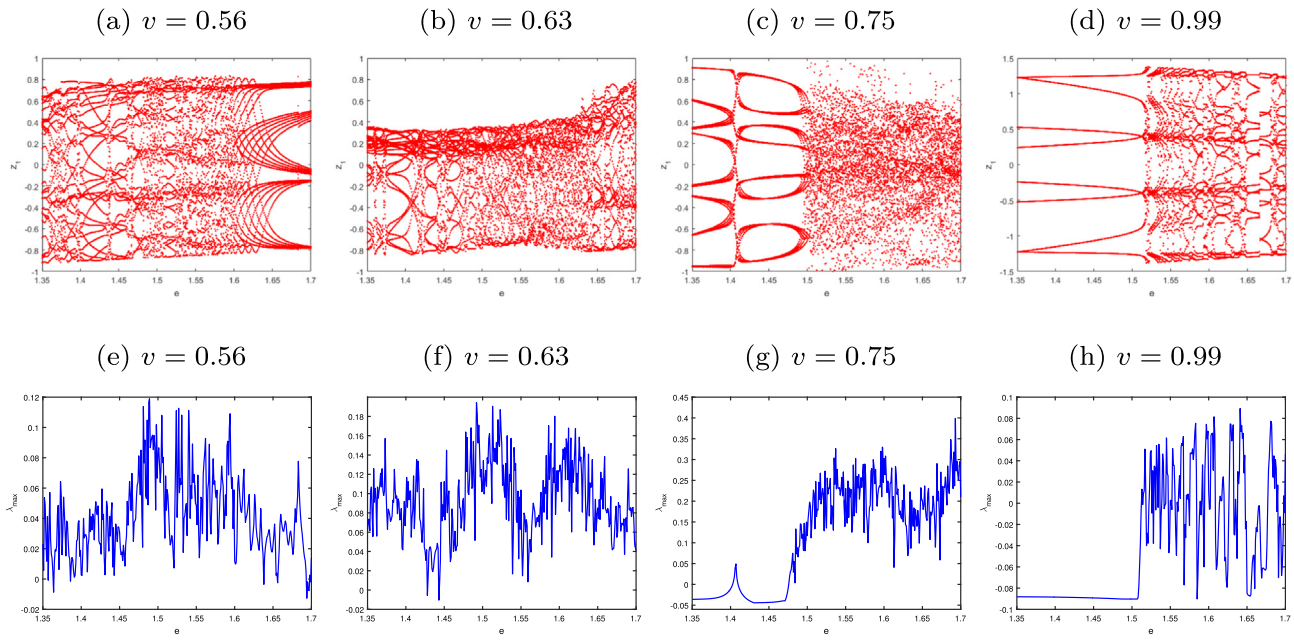

Fig. 2 The bifurcations and maximum Lyapunov exponents versus the parameter system e of the commensurate FDNN (1) for different fractional values ϑ.

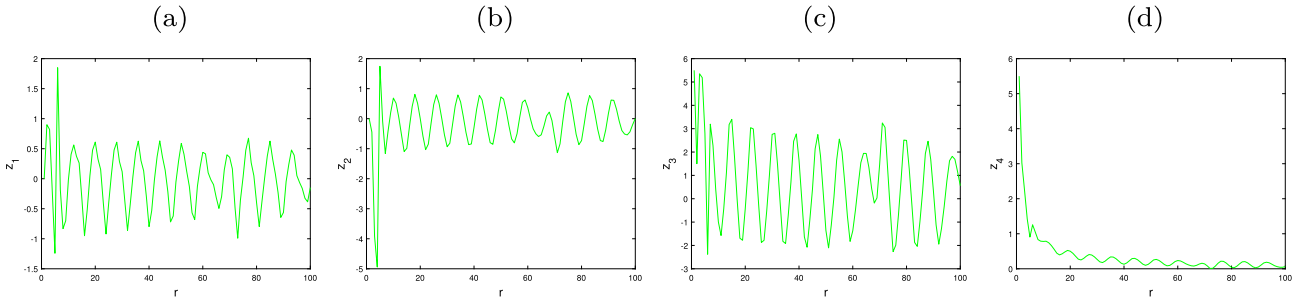

Fig. 3 Time evolution of (1) for $\vartheta = 0.75$ and $a_1 = 1.5, a_2 = 2, a_3 = 0.9, b_1 = -1.5, b_2 = 1.5, b_3 = -0.45, c_1 = 3, c_2 = -2, c_3 = 1.5, d_1 = 0.1, d_2 = -0.45, \alpha = -0.5, \beta = -0.12, e = 1.519$ and I.C.$(0, 0, 5.5, 5.5)$.

Case 1. We vary the order ϑ_1 from 0 to 1 with step size $\Delta\vartheta_1 = 0.001$. Figs. 6a and 6b illustrate the bifurcation and its corresponding maximum Lyapunov exponent for $\vartheta_2 = 1, \vartheta_3 = 1, \vartheta_4 = 0.9$, the parameter values $a_1 = 1.5, a_2 = 2, a_3 = 0.9, b_1 = -1.5, \quad b_2 = 1.5, b_3 = -0.45, \quad c_1 = 3, c_2 = -2, c_3 = 1.5, d_1 = 0.1, d_2 = -0.45, \alpha = -0.5, \beta = -0.12, e = 1.519$ and the I.C $(0, 0, 5.5, 5.5)$. It is clear that from Fig. 6a, the state of the incommensurate FDNN (9) displays chaotic behavior for smaller values of ϑ_1, as reflected by positive Lyapunov exponents, as seen in Fig. 6b. The λ_{max} shown in Fig. 1b changes between positive and negative for the fractional order value ϑ_1 close to 1. This result means a chaotic region is seen with the appearance of some periodic windows.

Case 2. The bifurcation and its λ_{max} are drawn in order to examine the dynamic behaviors of the incommensurate fractional neural network model (9) when ϑ_2 is an adjustable parameter, as displayed in Fig. 7. These results are obtained by varying ϑ_2 in the range $(0, 1]$ and with incommensurate orders $\vartheta_1 = 0.9, \vartheta_3 = 1$ and $\vartheta_4 = 0.9$. The initial conditions $(z_1(0), z_2(0), z_3(0), z_4(0)) = (0, 0, 5.5, 5.5)$, and the parameter values $a_1 = 1.5, a_2 = 2, a_3 = 0.9, b_1 = -1.5, \ b_2 = 1.5, b_3 = -0.45, c_1 = 3, c_2 = -2, c_3 = 1.5, d_1 = 0.1, d_2 = -0.45, \alpha = -0.5, \beta = -0.12, e = 1.519$ have remained unchanged. We can observe that when the order ϑ_2 takes small values, the trajectories become stable. When ϑ_2 increases, chaotic behaviors can be obtained where the values of λ_{max} are positive, and small periodic regions are also seen where the λ_{max} have negative values. Moreover, when ϑ_2 gets larger and approaches 1, the MLEs values change between positive and negative, meaning that the trajectories of the incommensurate FDNN model (9) change their motion from chaotic to periodic.

Case 3. We draw the bifurcation chart and its λ_{max} of the proposed new incommensurate FDNN model (9) versus $\vartheta_3 \in (0, 1]$ and we chose the incommensurate orders as $\vartheta_1 = 0.5, \vartheta_2 = 1$ and $\vartheta_4 = 1$. From Fig. 8, in con-

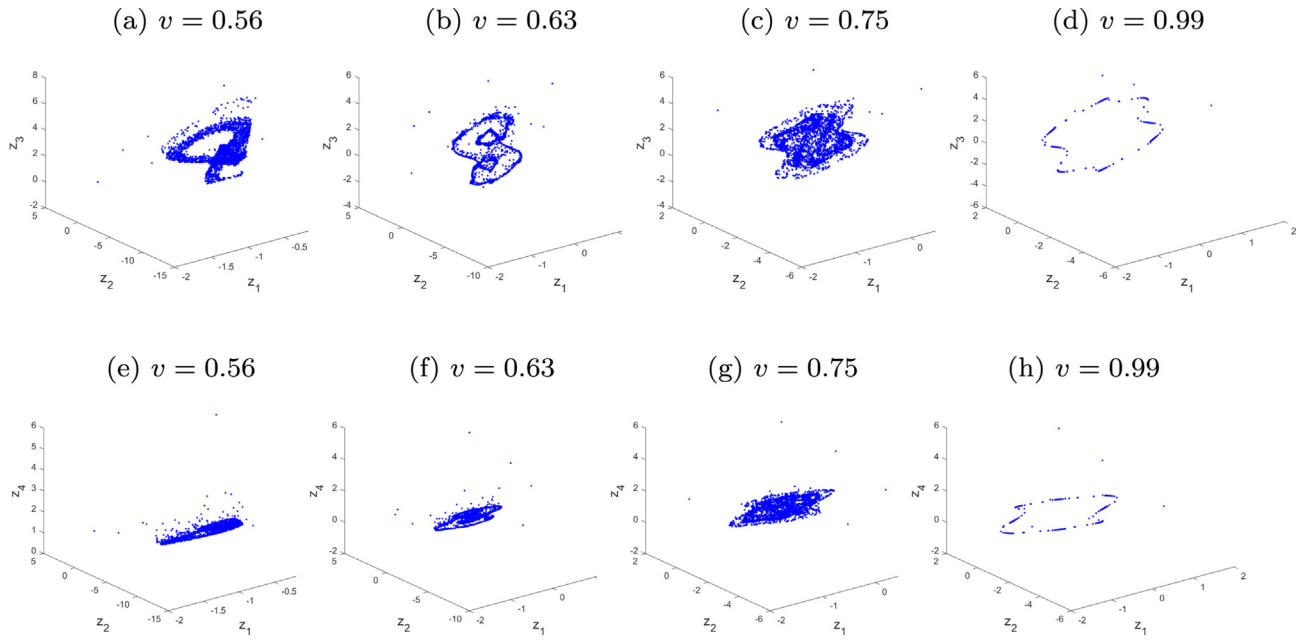

Fig. 4 Phase portraits of (1) for different values of ϑ.

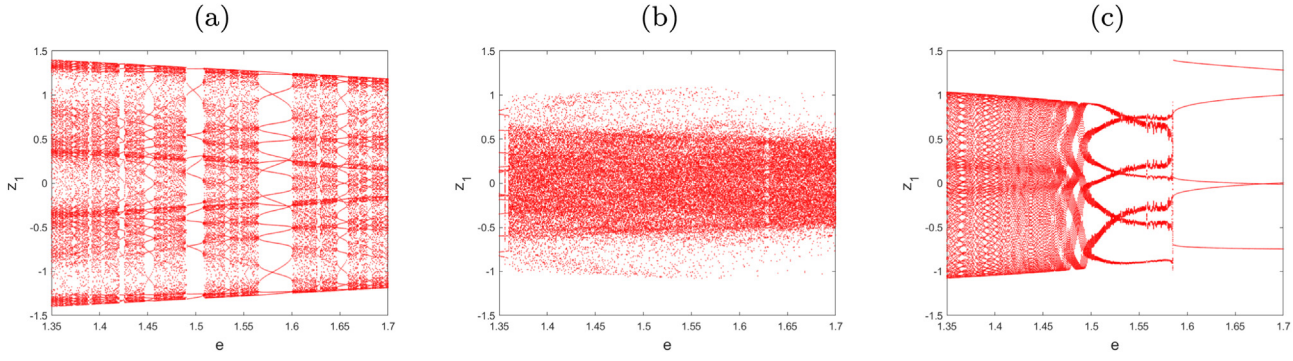

Fig. 5 Bifurcations of (9) versus the parameter system e for (a) $(\vartheta_1, \vartheta_2, \vartheta_3, \vartheta_4) = (0.9, 1, 1, 0.9)$ (b) $(\vartheta_1, \vartheta_2, \vartheta_3, \vartheta_4) = (0.9, 0.3, 1, 0.9)$ (c) $(\vartheta_1, \vartheta_2, \vartheta_3, \vartheta_4) = (0.5, 1, 0.7, 1)$.

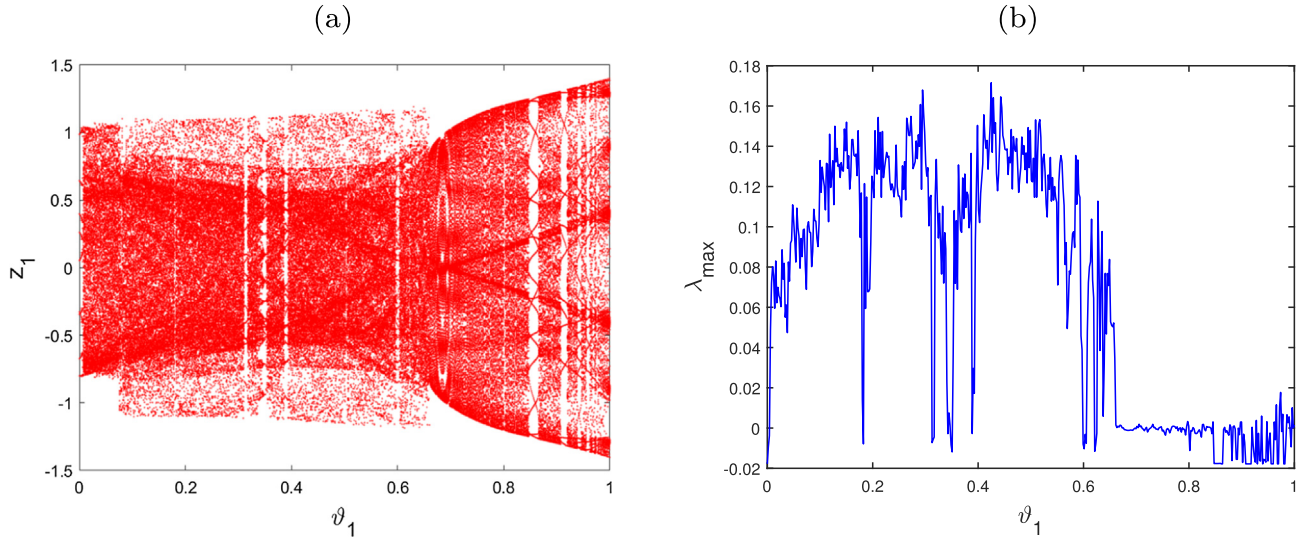

Fig. 6 Bifurcation of (9) and corresponding MLE versus the incommensurate fractional order ϑ_1 for $\vartheta_2 = 1, \vartheta_3 = 1$ and $\vartheta_4 = 0.9$.

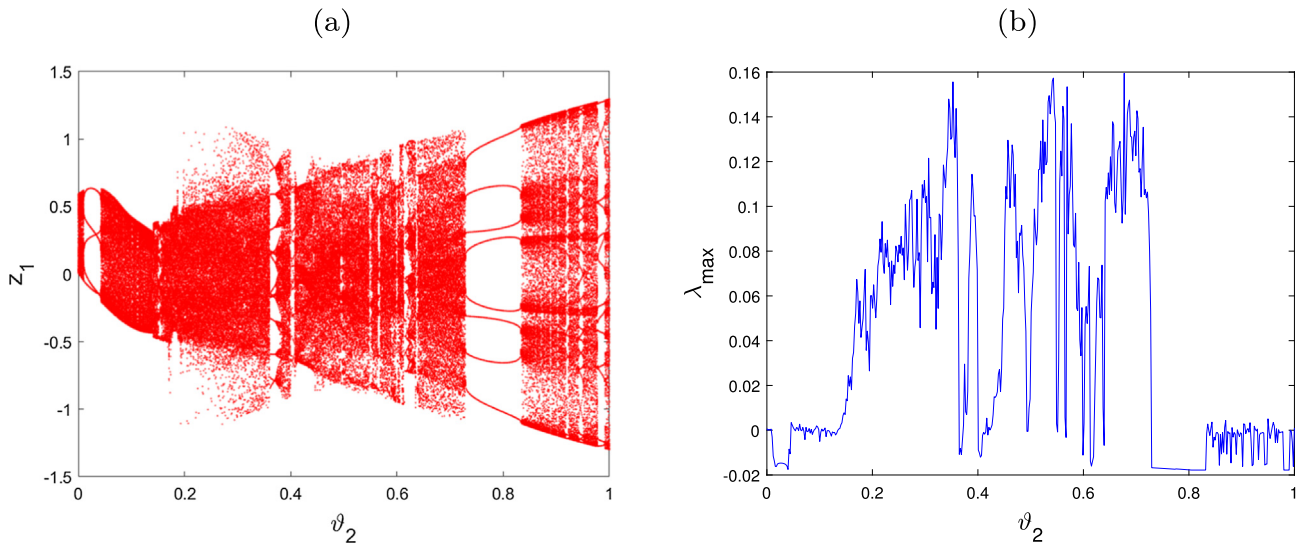

Fig. 7 Bifurcation of (9) and corresponding MLE versus the incommensurate fractional order ϑ_2 for $\vartheta_1 = 0.9, \vartheta_3 = 1$ and $\vartheta_4 = 0.9$.

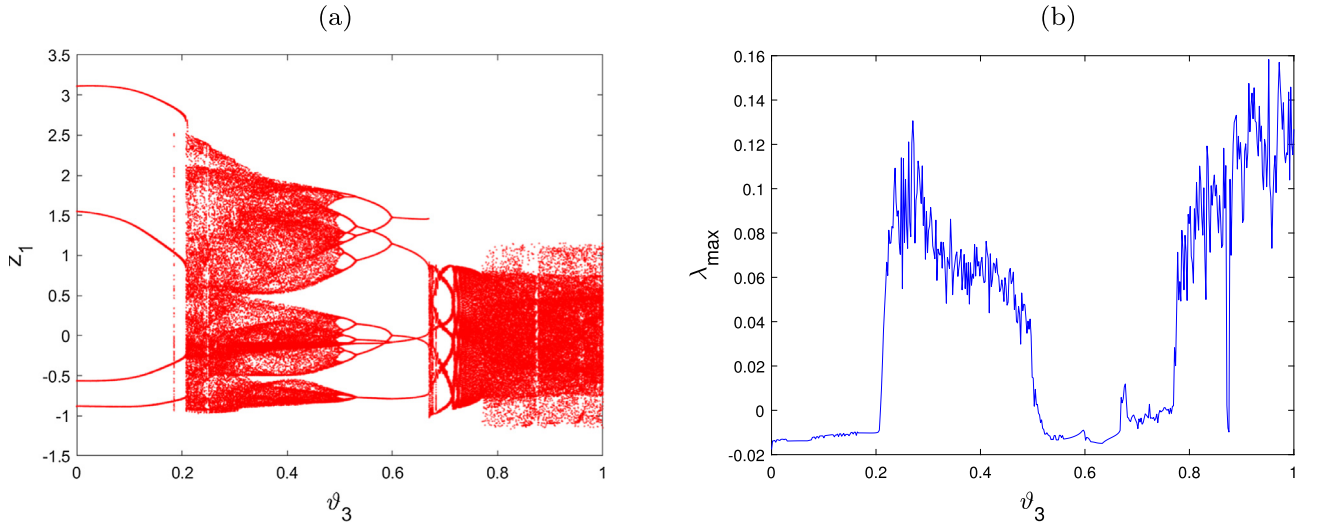

Fig. 8 Bifurcation of (9) and corresponding MLE versus the incommensurate fractional order ϑ_3 for $\vartheta_1 = 0.5, \vartheta_2 = 1$ and $\vartheta_4 = 1$.

trast to the previous cases, we observe that the trajectories of the incommensurate model are chaotic when the order ϑ_3 takes larger values and approaches 1 in which λ_{max} takes their highest value. the trajectories become stable. In addition, When ϑ_3 decreases, the stability region is shown and periodic windows appear. If the incommensurate order ϑ_3 decrease further, chaotic behaviors occur again in $\vartheta_3 \in (0.211, 0.509)$. When the order continues to decrease and close to zero, chaos disappears and periodic windows with four-period orbits are observed where the values of λ_{max} are negative. According to these findings, changes in the incommensurate orders have an effect on the dynamical properties of a fractional discrete neural network model with electromagnetic radiation (9). It also suggests that the system's behaviors may be more accurately represented by incommensurate orders, which is supported by the phase portraits of the state variables of the incommensurate fractional system (9) seen in Fig. 9.

3.3. Variable order FDNN model

The major goal of this section is to explore the complex dynamics of the FDNN MODEL with fractional variable order value. The variable order fractional discrete neural network model is represented as

$$\begin{cases} {}^{c}\Delta_{d}^{\vartheta(r)} z_1(r) = -z_1(r-1+\vartheta(r)) + a_1 \tanh(z_1(r-1+\vartheta(r))) + a_2 \tanh(z_2(r-1+\vartheta(r))) \\ \qquad +a_3 \tanh(z_3(r-1+\vartheta(r))), \\ {}^{c}\Delta_{d}^{\vartheta(r)} z_2(r) = -z_2(r-1+\vartheta(r)) + b_1 \tanh(z_1(r-1+\vartheta(r))) + b_2 \tanh(z_2(r-1+\vartheta(r))) \\ \qquad +b_3 \tanh(z_3(r-1+\vartheta(r))) + \alpha z_2(r-1+\vartheta(r)) \left(e + \beta (z_4(r-1+\vartheta(r)))^4\right), \\ {}^{c}\Delta_{d}^{\vartheta(r)} z_3(r) = -z_3(r-1+\vartheta(r)) + c_1 \tanh(z_1(r-1+\vartheta(r))) + c_2 \tanh(z_2(r-1+\vartheta(r))) \\ \qquad +c_3 \tanh(z_3(r-1+\vartheta(r))), \\ {}^{c}\Delta_{d}^{\vartheta(r)} z_4(r) = d_1 z_2(r-1+\vartheta(r)) + d_2 z_4(r-1+\vartheta(r)), \end{cases} \tag{11}$$

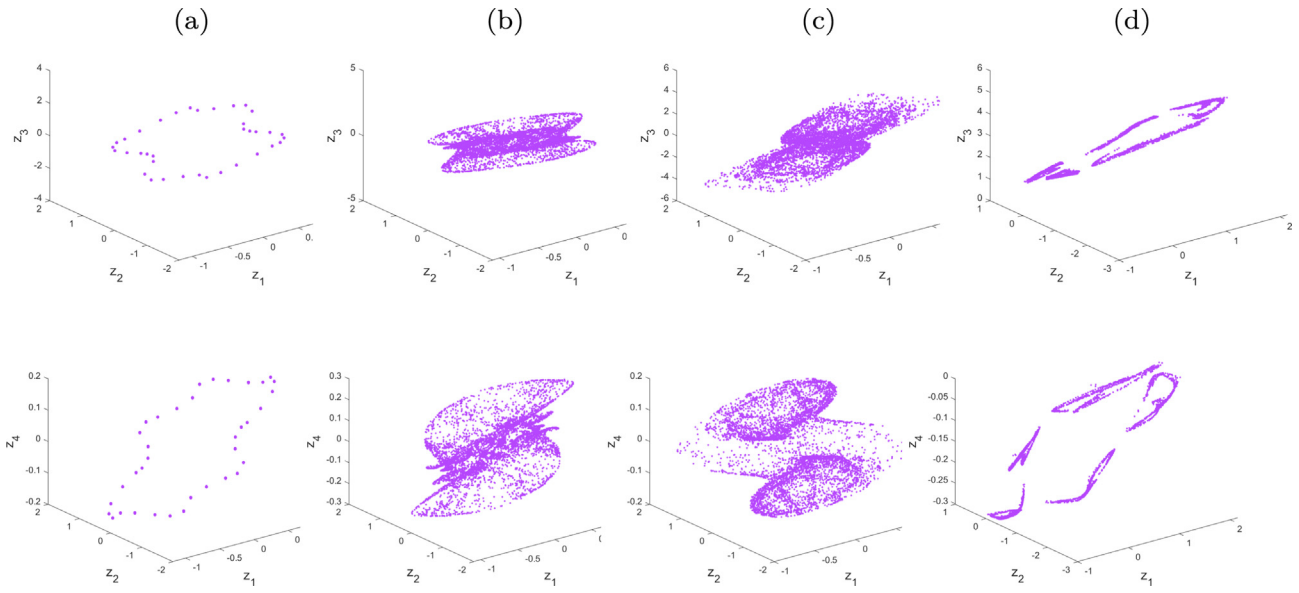

Fig. 9 Phase portraits of (9) for (a) $(\vartheta_1, \vartheta_2, \vartheta_3, \vartheta_4) = (0.8, 1, 1, 0.9)$ (b) $(\vartheta_1, \vartheta_2, \vartheta_3, \vartheta_4) = (0.1, 1, 1, 0.9)$ (c) $(\vartheta_1, \vartheta_2, \vartheta_3, \vartheta_4) = (0.9, 0.3, 1, 0.9)$ (d) $(\vartheta_1, \vartheta_2, \vartheta_3, \vartheta_4) = (0.5, 1, 0.3, 1)$.

where $r \in \mathbb{N}_{a+1-\vartheta(r)}, \vartheta(r) \in (0, 1]$ is the fractional variable order. The numerical model of the variable order FDNN model is derived from Lemma 1 as follows:

$$\begin{cases} z_1(r+1) = z_1(0) + \sum_{k=0}^{n} \frac{\Gamma(r-1-k+\vartheta(k))}{\Gamma(\vartheta(k))\Gamma(r-k)} \left(-z_1(k) + a_1 \tanh(z_1(k)) + a_2 \tanh(z_2(k)) \right. \\ \qquad \left. + a_3 \tanh(z_3(k))\right), \\ z_2(r+1) = z_2(0) + \sum_{k=0}^{n} \frac{\Gamma(r-1-k+\vartheta(k))}{\Gamma(\vartheta(k))\Gamma(r-k)} \left(-z_2(k) + b_1 \tanh(z_1(k)) + b_2 \tanh(z_2(k)) \right. \\ \qquad \left. + b_3 \tanh(z_3(k)) + \alpha z_2(k)\left(e + \beta(z_4(k))^4\right)\right), \\ z_3(r+1) = z_3(0) + \sum_{j=0}^{n} \frac{\Gamma(r-1-k+\vartheta(k))}{\Gamma(\vartheta(k))\Gamma(r-k)} \left(-z_3(k) + c_1 \tanh(z_1(k)) + c_2 \tanh(z_2(k)) \right. \\ \qquad \left. + c_3 \tanh(z_3(k))\right), \\ z_4(r+1) = z_4(0) + \sum_{j=0}^{n} \frac{\Gamma(r-1-k+\vartheta(k))}{\Gamma(\vartheta(k))\Gamma(r-k)} \left(d_1 z_2(k) + d_2 z_4(k)\right), \quad r = 1, 2, \cdots. \end{cases} \tag{12}$$

To illustrate the impact of the variable order on the behaviors of the FDNN (11), We set the system parameter $a_1 = 1.5, a_2 = 2, a_3 = 0.9, b_1 = -1.5, b_2 = 1.5, b_3 = -0.45$, $c_1 = 3, c_2 = -2, c_3 = 1.5, d_1 = 0.1, d_2 = -0.45$, $\alpha = -0.5, \beta = -0.12, e = 1.519$ and I.C.$(0, 0, 5.5, 5.5)$, Fig. 10 shows the resulting phase plots for different variable order. As can be observed in Fig. 10, the system (11) displays periodic behaviour for $v(r) = \frac{1}{12}\exp\left(\sin\left(\frac{r}{15}\right)\right) + 0.76$, and it displays chaotic behaviour for chosen fractional variable orders $v(r) = 0.7 + 0.2\frac{\exp(-r)}{1+\exp(-r)}$ and $v(r) = 0.7 + \frac{\exp(-r)}{1+\exp(-r)}$ but the shape of the attractors differ from a fractional variable order to another and the attractors are extremely different from those obtained in Fig. 4 These results can prove that the choice of the fractional variable order influences on the shape of the attractors of the system (11).

Since the phase plots are not definitive to describe the nature of the dynamics of the system, we are going to observe the bifurcation and the maximum Lyapunov exponents plots concerning the parameter $e \in [1.35, 1.7]$ to give more precise details on the dynamics of the system (11). We draw bifurcations and its λ_{max} for three different fractional variable orders $\vartheta(r) = \frac{1}{12}\exp\left(\sin\left(\frac{r}{15}\right)\right) + 0.76, \vartheta(r) = 0.7 + 0.2\frac{\exp(-r)}{1+\exp(-r)}$ and $\vartheta(r) = 0.7 + \frac{\exp(-r)}{1+\exp(-r)}$ as illustrated in Fig. 11. When looking at Fig. 11, It is easy to observe that the shape of the bifurcation diagrams is different for the three proposed fractional variable orders. In addition, when we change the value of the variable order $\vartheta(r)$, the stability region shrink and the chaotic region expand. For example, for $\vartheta(r) = \frac{1}{12}\exp\left(\sin\left(\frac{r}{15}\right)\right) + 0.76$, the system is stable at first, and as the value of e increases, it gradually loses its stability and chaotic trajectories emerge. For $\vartheta(r) = 0.7 + 0.2\frac{\exp(-r)}{1+\exp(-r)}$, the system becomes more chaotic, and the region in which the states are stable shrinks, whereas for $\vartheta(r) = 0.7 + \frac{\exp(-r)}{1+\exp(-r)}$, the chaos appears in all interval when $e \in [1.35, 1.7]$ except for some crisis points. Moreover, as compared with the results of the commensurate FDNN model (1) shown in Fig. 2 and the results of the incommensurate FDNN model (9) shown in Fig. 7, we notice that the diagrams are strictly different, which indicates that the choice of the fractional variable order affects the dynamic characteristics of the fractional discrete neural network model.

4. The 0–1 test for chaos and the Complexity analysis of the FDNN model

In this section, we analyze the complexity of the chaotic behaviors for evaluating the dynamic properties of chaotic systems in which the higher the amount of complexity, the more chaotic the system gets. Here, the complexity of the proposed fractional discrete neural network model is evaluated using the approximate entropy test as well as the C_0 complexity algorithm. Also, we will use the 0–1 method to confirm the presence of chaos in the FDNN model.

4.1. The 0–1 test of the FDNN model

Here, we will employ the 0–1 test approach, which was provided by Gottwald and Melbourne [49], in order to detect

$$v(r) = \frac{1}{12}\exp(\sin(\frac{r}{15})) + 0.76$$

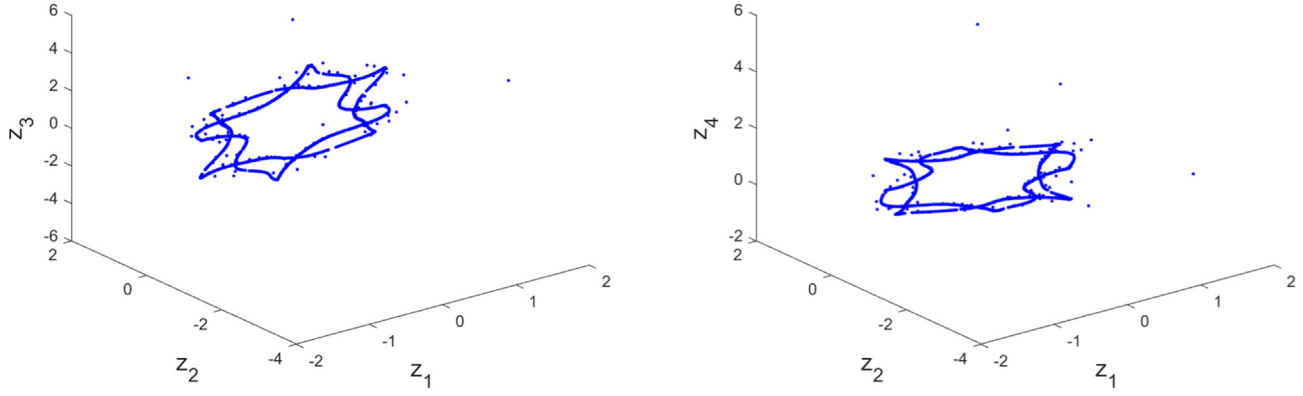

$$v(r) = 0.7 + 0.2\frac{\exp(-r)}{1+\exp(-r)}$$

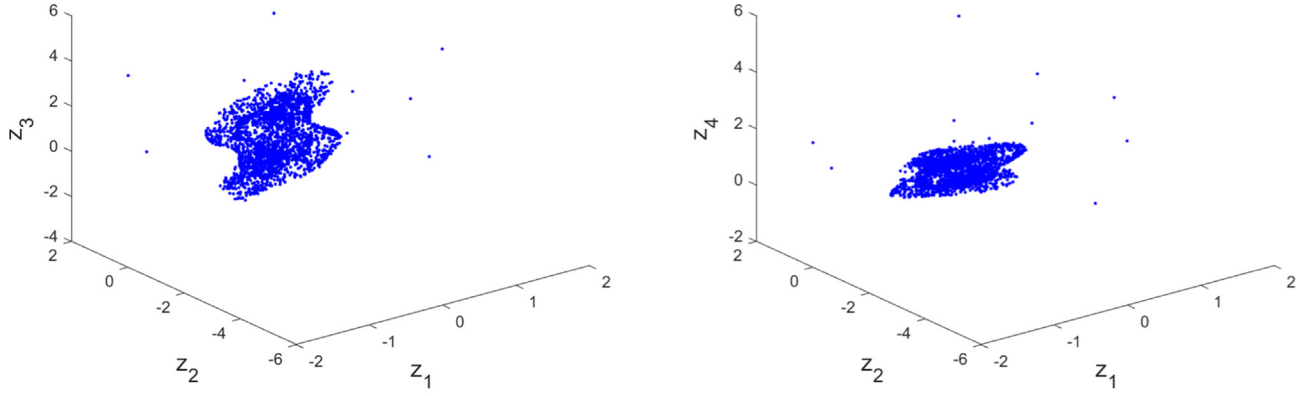

$$v(r) = 0.7 + \frac{\exp(-r)}{1+\exp(-r)}$$

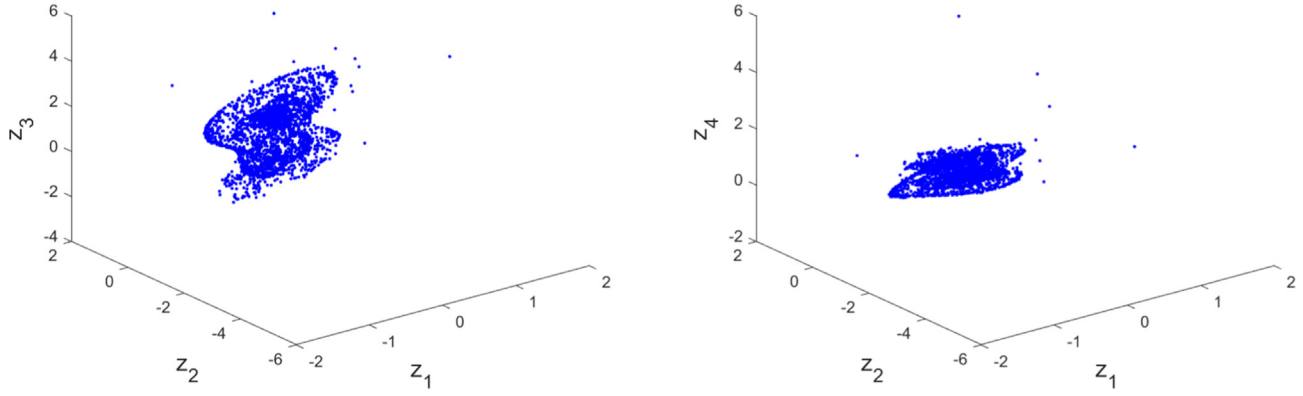

Fig. 10 Phase portraits of the variable order FDNN (11) for different variable values of $\vartheta(r)$.

$$v(r) = \frac{1}{12}\exp(\sin(\frac{r}{15})) + 0.76$$

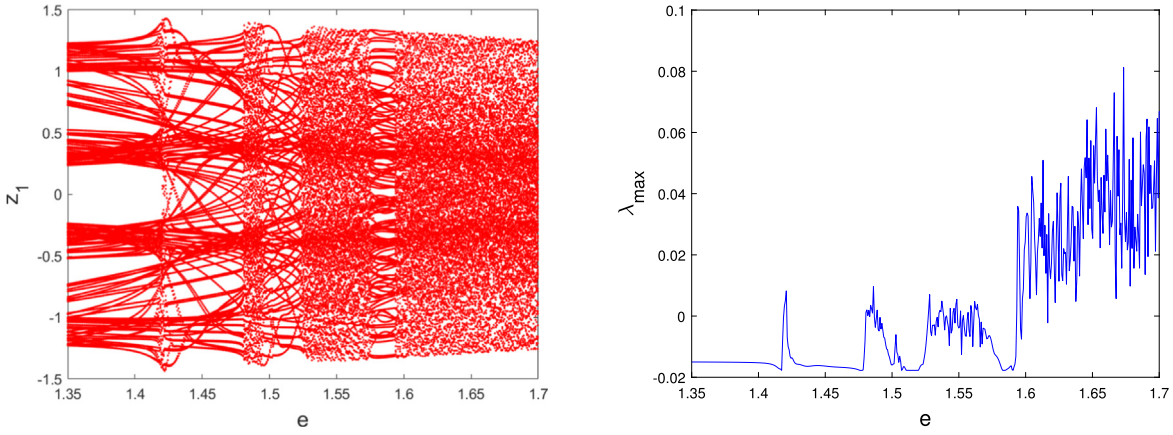

$$v(r) = 0.7 + 0.2\frac{\exp(-r)}{1+\exp(-r)}$$

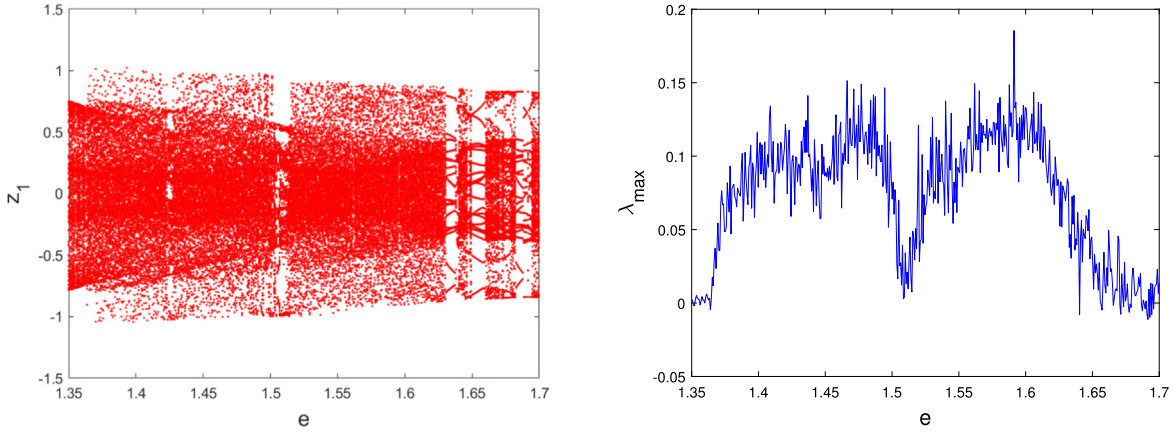

$$v(r) = 0.7 + \frac{\exp(-r)}{1+\exp(-r)}$$

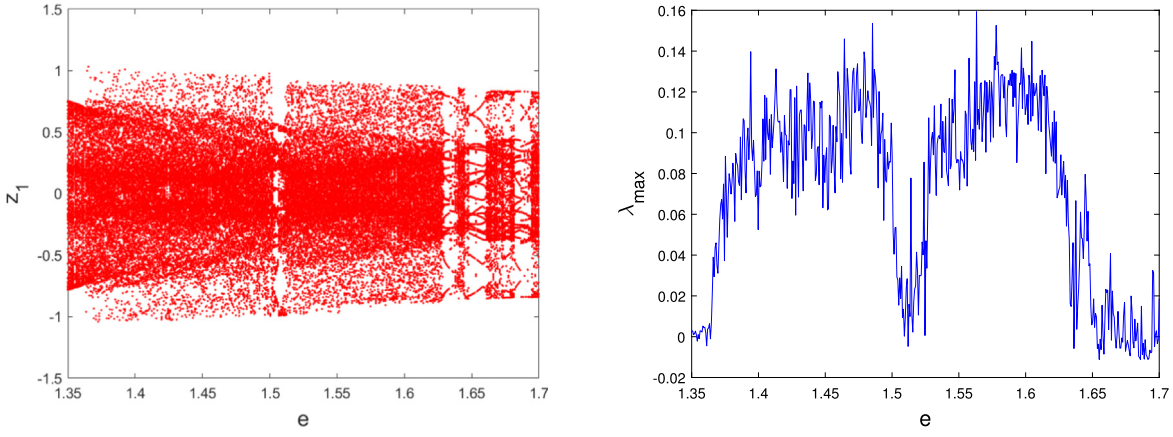

Fig. 11 The bifurcations maximum Lyapunov exponents versus the parameter system e of the variable order FDNN (11) for different fractional variable values $\vartheta(r)$.

the difference between chaotic and regular behaviors in dynamic systems. We take the series data as input, and if the dynamics of the model are chaotic, the output will be close to 1, otherwise, it will be close to 0. Furthermore, we describe the test as follows:

Firstly, by using the time series $(z_1(m))_{m=1,\ldots,N}$, we establish the translation variables as follows:

$$p_\varsigma(k)=\sum_{m=1}^{k} z_1(m)cos(i\varsigma),\ q_\varsigma(k)=\sum_{m=1}^{k} z_1(m)sin(i\varsigma), k=1,2,\ldots,N. \tag{13}$$

The $(p_\varsigma - q_\varsigma)$ chart is used to detect whether or not chaotic behaviours of the proposed FDNN model occur. If the trajectories of p_ς and q_ς are bounded, the dynamical behaviours of the model are regular, but if they indicate Brownian-like behaviour, the system's dynamics are chaotic. Furthermore, we introduce the mean square displacement formula as follows:

$$M_\varsigma(k)=\frac{1}{N}\sum_{m=1}^{N}\Big[\big(p_\varsigma(m+k)-p_\varsigma(m)\big)^2+\big(q_\varsigma(m+k)-q_\varsigma(m)\big)^2\Big],\quad k\leqslant\frac{N}{10}. \tag{14}$$

Finally, we represent the asymptotic growth by:

$$K_\varsigma=\lim_{k\to\infty}\frac{\log M_\varsigma}{\log k}. \tag{15}$$

The growth rate "$K=\text{median}(K_\varsigma)$" allows the distinction between nonchaotic and chaotic motions in the proposed commensurate FDNN model (1). If K is closer to, this suggests that the model is not chaotic, whereas if K is closer to 1, the model is chaotic.

Fig. 12 illustrates the results of asymptotic growth rate K of the commensurate FDNN model (1) for $\vartheta\in[0.5,1]$ in which $e=1.519$ and $e=1.65$. We can show that when the parameter e decreases, the growth rate K approaches 1 which proves that the commensurate FDNN model (1) has chaotic behaviour and it clearly confirms the previous results of bifurcations and their λ_{max} shown in Fig. 2. Now, to validate the occurrence of chaos in the incommensurate order FDNN model (9) and the variable order FDNN model (11), the results of the $p-q$ plots for different incommensurate values and variable values are depicted in Figs. 13 and 14, respectively. It is evident that Figs. 13a and 14a show bounded trajectories, which indicates that the system is periodic. In contrast, Figs. 13b, 13c, 14b and 14c display Brownian-like trajectories, which confirm the occurrence of chaotic motions in the incommensurate FDNN model and the variable FDNN model.

4.2. The ApEn of the FDNN model

Now, we describe the complexity of the fractional neural network system (1) by using the approximate entropy (ApEn) algorithm [50]. The ApEn is a measure of complexity of systems generated by a time series. Note that a time series with a higher values of ApEn are more complex ones. To calculate ApEn, we define first $n-m+1$ vectors as follows:

$$Z(i)=[z(i),\ldots,z(i+m-1)], \tag{16}$$

for $i\in[1,n-m+1]$ where $z(1),z(2),\ldots,z(n)$ is a set of discrete points. In addition, we discribe the following equation:

$$C_i^m(r)=\frac{K}{n-m+1}, \tag{17}$$

where K is the number of $Z(i)$ having $d(Z(i),Z(j))\leqslant r$. Note that the value of the approximate entropy depends on two important parameters: the similar tolerance r and the embedding dimension m. Here, we set $m=2$ and $r=0.2std(Z)$ where $std(Z)$ is the standard deviation of the data Z. Theoretically, the ApEn is calculated as:

$$ApEn=\phi^m(r)-\phi^{m+1}(r), \tag{18}$$

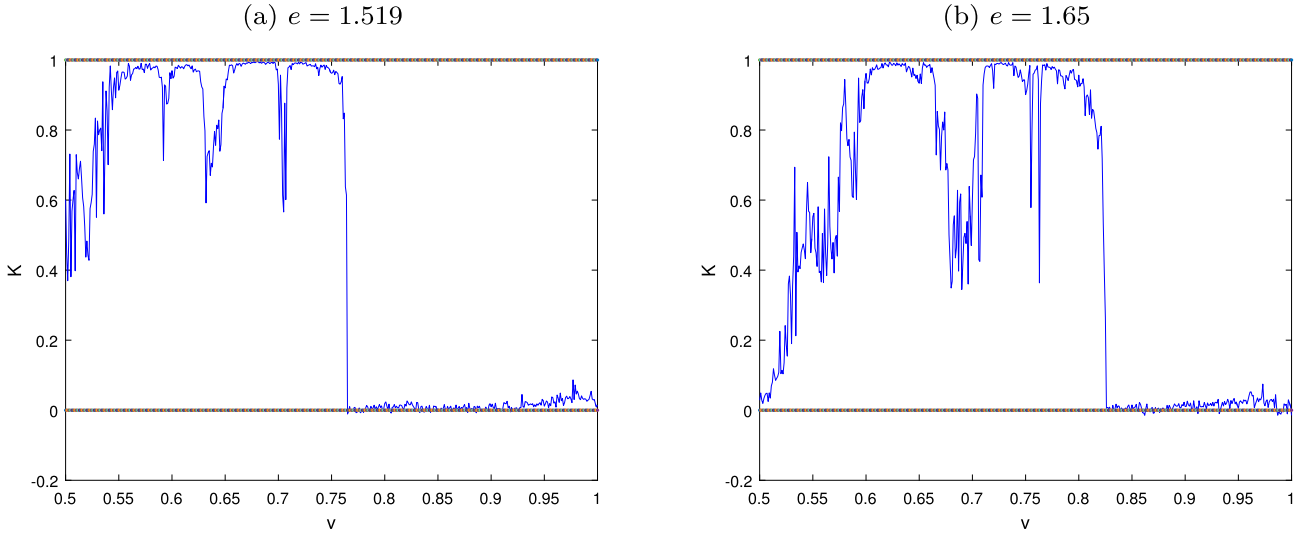

Fig. 12 he 0–1 test versus the fractional order ϑ of the commensurate FDNN model (1) for $a_1=1.5, a_2=2, a_3=0.9, b_1=-1.5, b_2=1.5, b_3=-0.45, c_1=3, c_2=-2, c_3=1.5, d_1=0.1, d_2=-0.45, \alpha=-0.5, \beta=-0.12, e=1.519,\ 1.65$ and I.C.$(0,0,5.5,5.5)$.

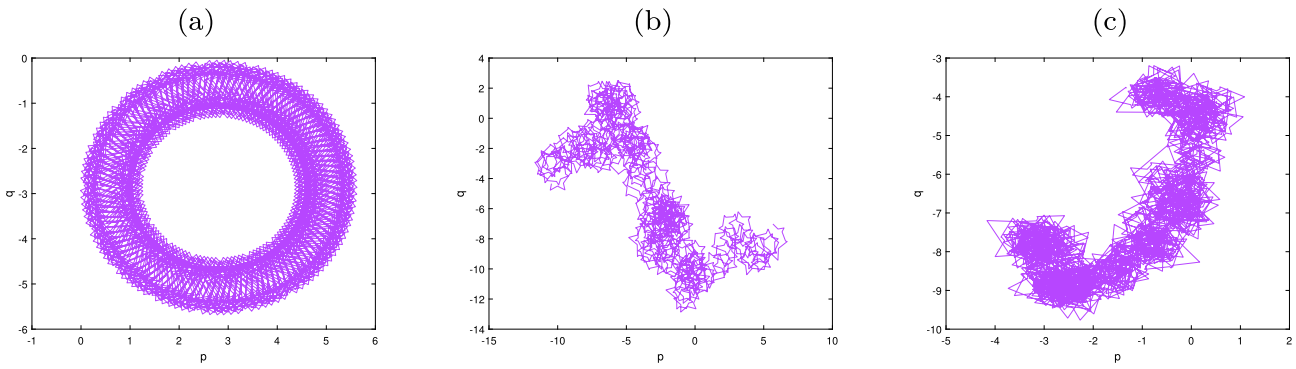

Fig. 13 The $(p-q)$ plots of the incommensurate FDNN model (9) for (a) $(\vartheta_1,\vartheta_2,\vartheta_3,\vartheta_4)=(0.8,1,1,0.9)$ (b) $(\vartheta_1,\vartheta_2,\vartheta_3,\vartheta_4)=(0.9,0.3,1,0.9)$ (c) $(\vartheta_1,\vartheta_2,\vartheta_3,\vartheta_4)=(0.5,1,0.3,1)$.

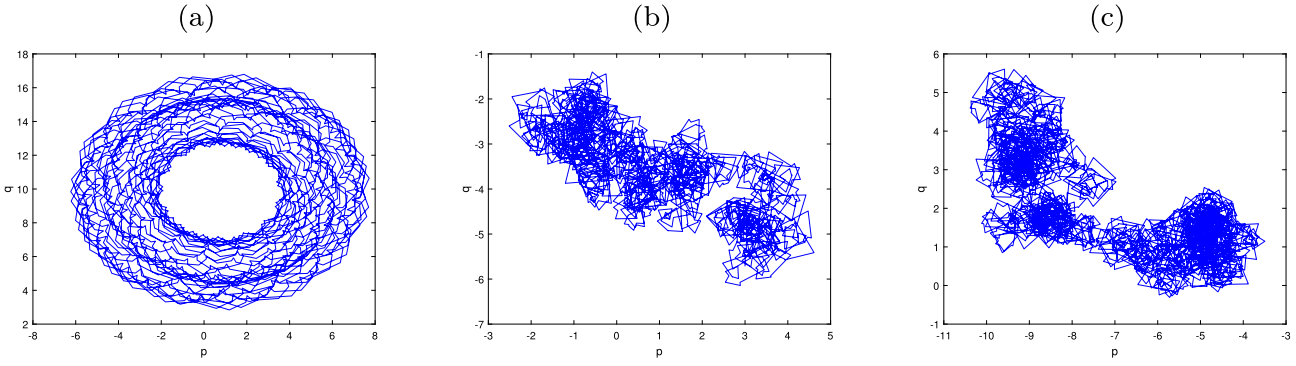

Fig. 14 The $(p-q)$ plots of the variable FDNN model (11) for (a) $\vartheta(r)=\frac{1}{12}\exp\left(\sin\left(\frac{r}{15}\right)\right)+0.76$, (b) $\vartheta(r)=0.7+0.2\frac{\exp(-r)}{1+\exp(-r)}$, (c) $\vartheta(r)=0.7+\frac{\exp(-r)}{1+\exp(-r)}$.

where,

$$\phi^m(r)=\frac{1}{n-m-1}\sum_{i=0}^{n-m+1}\log C_i^m(r). \tag{19}$$

Setting the parameters $a_1=1.5, a_2=2, a_3=0.9, b_1=-1.5, b_2=1.5, b_3=-0.45, c_1=3, c_2=-2, c_3=1.5,\ d_1=0.1, d_2=-0.45, \alpha=-0.5, \beta=-0.12$ and I.C.$(0,0,5.5,5.5)$, the approximate entropy results of the commensurate FDNN model (1), the incommensurate FDNN model (9) and the variable order FDNN model (11) are given in Figs. 15a, 15b and 15c, respectively. It is clear that in order to acquire larger values of ApEn, the time series has a higher level of complexity. As a consequence, these findings are in accordance with the MLE results that were shown before, which therefore validates the presence of chaos in the proposed fractional system.

4.3. The C_0 complexity of the FDNN model

In this part, we use the C0 complexity method based on the inverse Fourier transform to figure out the complexity of the suggested fractional discrete neural network system. The following is the description of the algorithm[51,52]:

For a sequence $\phi(0),\ldots,\phi(M-1)$, the algorithm of the C_0 complexity is given as follows:

1. We compute the Fourier transform of the sequence $x(m)$ by:

$$Z_N(l)=\frac{1}{N}\sum_{l=0}^{N-1}x(l)\exp^{-2\pi i\left(\frac{kl}{N}\right)},\quad l=0,1,..,N-1. \tag{20}$$

2. We figure out the mean square by: $G_N=\frac{1}{N}\sum_{l=0}^{N-1}|Z_N(l)|^2$and we define

$$\overline{Z}_N(l)=\begin{cases} Z_N(l) & \text{if}\quad \|Z_N(l)\|^2>rG_N,\\ 0 & \text{if}\quad \|Z_N(l)\|^2\leqslant rG_N.\end{cases} \tag{21}$$

3. We determine the inverse Fourier transform using the following formula:

$$\xi(\imath)=\frac{1}{N}\sum_{l=0}^{N-1}\bar{z}_N(l)\exp^{2\pi i\left(\frac{\imath l}{N}\right)},\quad \imath=0,1,..,N-1. \tag{22}$$

4. The complexity of C_0 is figured out by using the following formula:

$$C_0=\frac{\sum_{\imath=0}^{N-1}\|\xi(\imath)-x(\imath)\|}{\sum_{\imath=0}^{N-1}\|x(\imath)\|^2}. \tag{23}$$

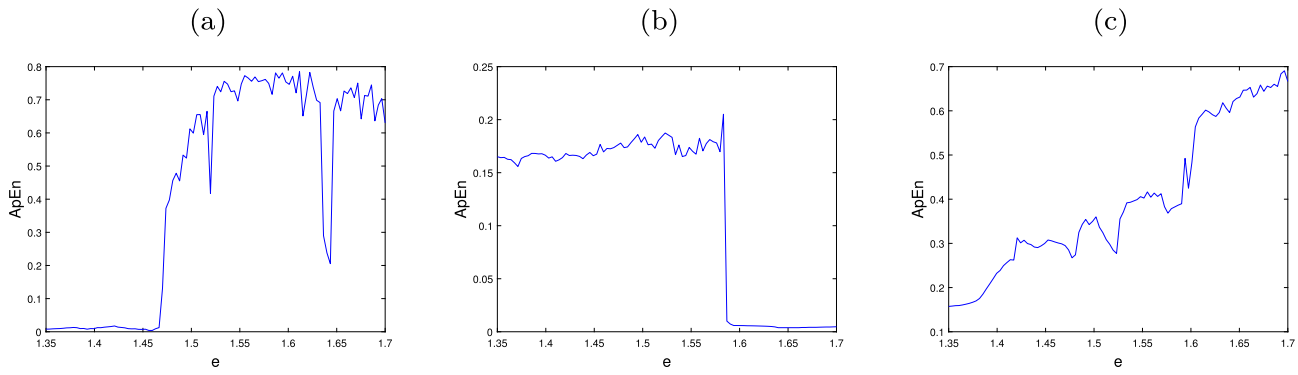

Fig. 15 The ApEn of the FDNN model versus the parameter e for (a) $\vartheta = 0.99$, (b) $(\vartheta_1, \vartheta_2, \vartheta_3, \vartheta_4) = (0.5, 1, 0.7, 1)$, (c) $v(r) = \frac{1}{12}\exp\left(\sin\left(\frac{r}{15}\right)\right) + 0.76$.

The C_0 complexity of the commensurate FDNN model (1) is shown in Fig. 16a. Fig. 16b illustrates the results of estimating the C_0 complexity of the incommensurate FDNN model (9) and the C_0 results of the variable order FDNN model (11) is displayed if Fig. 16c. We get these results by adjusting the system parameters $a_1 = 1.5, a_2 = 2, a_3 = 0.9, b_1 = -1.5, b_2 = 1.5, b_3 = -0.45, c_1 = 3, c_2 = -2, c_3 = 1.5, d_1 = 0.1, d_2 = -0.45$, $\alpha = -0.5, \beta = -0.12$, the initial conditions $(z_1(0), z_2(0), z_3(0), z_4(0)) = (0, 0, 5.5, 5.5)$ and varying the system parameter $e \in [1.35, 1.7]$. From Fig. 16a, as with MLE, the C_0 values of the commensurate system (1) increase as the parameter e decreases. Furthermore, when $(\vartheta_1, \vartheta_2, \vartheta_3, \vartheta_4) = (0.5, 1, 0.7, 1)$, the incommensurate system (9) exhibits lower complexity when the values of e increase and close to 1.7, which is compatible with the findings of the bifurcation and the approximate entropy test (ApEn). Besides, from Fig. 16c, the greater complexity of the variable order system (11) is noticed in the interval where the parameter e increases. Thus, we can infer that the C_0 complexity measure is a reliable means of quantifying complexity effectively.

5. The control of the fractional discrete neural network model

5.1. Stabilisation of FDNN model

In this section, we suggest a stabilization controller to stabilize the chaotic trajectories of the proposed fractional discrete neural network model. The goal of the stabilization control problem is to design a good adaptive controller that makes all of the system's states tend asymptotically to zero. To this aim, we first recall the Lemma of the stability of fractional map.

Lemma 2. [53]Let $z(r) = (z_1(r), \ldots, z_n(r))^T$ and $B \in \mathscr{M}_n(\mathbb{R})$. The zero fixed point of the linear fractional order discrete system

$$ {}^{c}\Delta_d^{\vartheta} z(r) = B\, z(r - 1 + \vartheta), \tag{24}$$

$\forall\ r \in \mathbb{N}_{d+1-\vartheta}$ is asymptotically stable if

$$\lambda_\iota \in \left\{ \gamma \in \mathbb{C} : |\ \vartheta\ | < \left(2\cos\frac{|\ \arg\gamma\ | - \pi}{2 - \vartheta}\right)^{\vartheta} \quad \text{and} \quad |\ \arg\vartheta\ | > \frac{\vartheta\ \pi}{2} \right\}, \tag{25}$$

where λ_ι are the eigenvalues of the matrix B.

Now, the controlled FDNN system is given by:

$$\begin{cases} {}^{c}\Delta_d^{\vartheta} z_1(r) = -z_1(r-1+\vartheta) + a_1 \tanh(z_1(r-1+\vartheta)) + a_2 \tanh(z_2(r-1+\vartheta)) \\ \qquad\qquad +a_3 \tanh(z_3(r-1+\vartheta)) + u_{z_1}(r-1+\vartheta), \\ {}^{c}\Delta_d^{\vartheta} z_2(r) = -z_2(r-1+\vartheta) + b_1 \tanh(z_1(r-1+\vartheta)) + b_2 \tanh(z_2(r-1+\vartheta)) \\ \qquad\qquad +b_3 \tanh(z_3(r-1+\vartheta)) + \alpha z_2(r-1+\vartheta)\left(e + \beta(z_4(r-1+\vartheta))^4\right) \\ \qquad\qquad +u_{z_2}(r-1+\vartheta), \\ {}^{c}\Delta_d^{\vartheta} z_3(r) = -z_3(r-1+\vartheta) + c_1 \tanh(z_1(r-1+\vartheta)) + c_2 \tanh(z_2(r-1+\vartheta)) \\ \qquad\qquad +c_3 \tanh(z_3(r-1+\vartheta)) + u_{z_3}(r-1+\vartheta), \\ {}^{c}\Delta_d^{\vartheta} z_4(r) = d_1 z_2(r-1+\vartheta) + d_2 z_4(r-1+\vartheta_4) + u_{z_4}(r-1+\vartheta), \end{cases} \tag{26}$$

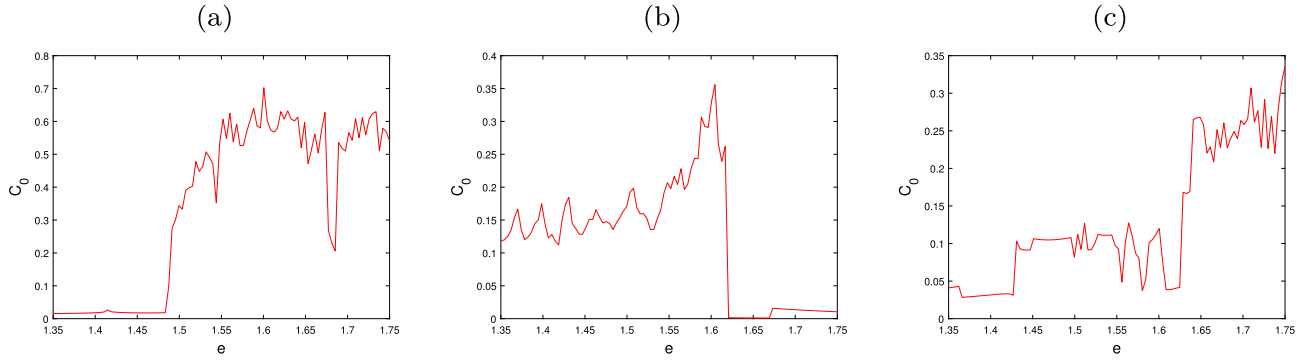

Fig. 16 The C_0 complexity of the FDNN model versus the parameter e for (a) $\vartheta = 0.99$, (b) $(\vartheta_1, \vartheta_2, \vartheta_3, \vartheta_4) = (0.5, 1, 0.7, 1)$, (c) $v(r) = \frac{1}{12}\exp\left(\sin\left(\frac{r}{15}\right)\right) + 0.76$.

where $u_{z_1}(r), u_{z_2}(t), u_{z_3}(r), u_{z_4}(r)$ and are the adaptive control terms. The proposed control law is represented in the following Theorem.

Theorem 1. The FDNN model (1) is stabilized subject to the following control law:

$$\begin{cases} u_{z_1}(r) = -a_1 \tanh(z_1(r)) - a_2 \tanh(z_2(r)) - a_3 \tanh(z_3(r)), \\ u_{z_2}(r) = -b_1 \tanh(z_1(r)) - b_2 \tanh(z_2(r)) - b_3 \tanh(z_3(r)) - \alpha z_2(r)\big(e + \beta z_4^4(r)\big), \\ u_{z_3}(r) = -c_1 \tanh(z_1(r)) - c_2 \tanh(z_2(r)) - c_3 \tanh(z_3(r)), \\ u_{z_4}(r) = -d_1 z_2(r). \end{cases} \tag{27}$$

Proof. By substituting (27) into (26), we get the following system:

$$\begin{cases} {}^c\Delta_d^{\vartheta} z_1(r) = -z_1(r-1+\vartheta), \\ {}^c\Delta_d^{\vartheta} z_2(r) = -z_2(r-1+\vartheta), \\ {}^c\Delta_d^{\vartheta} z_3(r) = -z_3(r-1+\vartheta), \\ {}^c\Delta_d^{\vartheta} z_4(r) = d_2 z_4(r-1+\vartheta). \end{cases} \tag{28}$$

which can be written as follows:

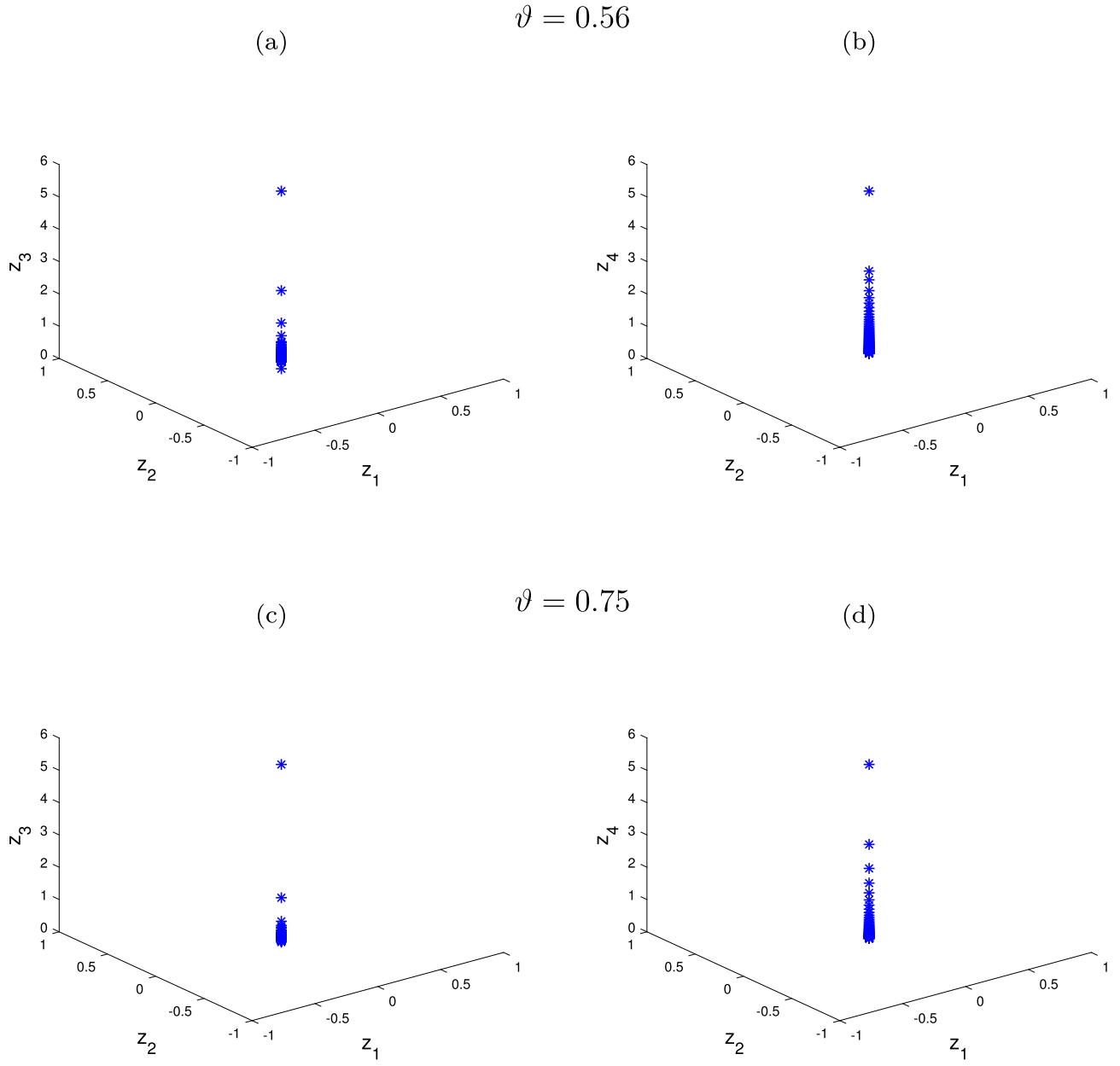

Fig. 17 Attractors of the controlled FDNN model (28) for $a_1 = 1.5, a_2 = 2, a_3 = 0.9, b_1 = -1.5, b_2 = 1.5, b_3 = -0.45, c_1 = 3, c_2 = -2, c_3 = 1.5, d_1 = 0.1, d_2 = -0.45, \alpha = -0.5, \beta = -0.12, e = 1.519$ and I.C.$(0, 0, 5.5, 5.5)$.

$$
\begin{aligned}
&{}^{c}\Delta_{d}^{\vartheta_1}\left(z_1(r), z_2(r), z_3(r), z_4(r)\right)^T \\
&\quad = B(z_1(r), z_2(r), z_3(r), z_4(r))^T,
\end{aligned} \tag{29}
$$

where:

$$
B = \begin{pmatrix} -1 & 0 & 0 & 0 \\ 0 & -1 & 0 & 0 \\ 0 & 0 & -1 & 0 \\ 0 & 0 & 0 & d_2 \end{pmatrix}.
$$

The eigenvalues of the matrix B are $\lambda_1 = \lambda_2 = \lambda_3 = -1$, and $\lambda_4 = d_2$ where $d_2 = -0.45$, it is easy to see that the eigenvalues λ_j $(j = 1, 2, 3, 4)$ satisfies the condition of Lemma 2, which proves that the zero equilibrium of the controlled system (28) is asymptotically stable, therefore the states of the controlled system (28) are asymptotically stabilized.

The result of Theorem 1 are illustrated in Fig. 17 and Fig. 18 for $a_1 = 1.5, a_2 = 2, a_3 = 0.9, b_1 = -1.5, b_2 = 1.5, b_3 = -0.45$, $c_1 = 3, c_2 = -2, c_3 = 1.5, d_1 = 0.1$, $d_2 = -0.45$, $\alpha = -0.5$, $\beta = -0.12, e = 1.519$ and I.C.$(0, 0, 5.5, 5.5)$. Clearly, the states of the controlled system converge to zero and the chaotic nature of the system is deleted.

5.2. Synchronization scheme of FDNN model

This section presents an adaptive controller to synchronize the suggested FDNN model with electromagnetic radiation (1). The aim of the synchronization process is to force the error between the slave and the master systems to converge toward zero.

Let's consider the commensurate fractional system (1) as the master system:

$$
\begin{cases}
{}^{c}\Delta_{d}^{\vartheta} z_{1m}(r) = -z_{1m}(r-1+\vartheta) + a_1 \tanh(z_{1m}(r-1+\vartheta)) + a_2 \tanh(z_{2m}(r-1+\vartheta)) \\
\qquad\qquad +a_3 \tanh(z_{3m}(r-1+\vartheta)), \\
{}^{c}\Delta_{d}^{\vartheta} z_{2m}(r) = -z_{2m}(r-1+\vartheta) + b_1 \tanh(z_{1m}(r-1+\vartheta)) + b_2 \tanh(z_{2m}(r-1+\vartheta)) \\
\qquad\qquad +b_3 \tanh(z_{3m}(r-1+\vartheta)) + \alpha z_{2m}(r-1+\vartheta)\left(e + \beta(z_{4m}(r-1+\vartheta))^4\right), \\
{}^{c}\Delta_{d}^{\vartheta} z_{3m}(r) = -z_{3m}(r-1+\vartheta) + c_1 \tanh(z_{1m}(r-1+\vartheta)) + c_2 \tanh(z_{2m}(r-1+\vartheta)) \\
\qquad\qquad +c_3 \tanh(z_{3m}(r-1+\vartheta)), \\
{}^{c}\Delta_{d}^{\vartheta} z_{4m}(r) = d_1 z_{2m}(r-1+\vartheta) + d_2 z_{4m}(r-1+\vartheta).
\end{cases} \tag{30}
$$

Define the slave system as:

$$
\begin{cases}
{}^{c}\Delta_{d}^{\vartheta} z_{1s}(r) = -z_{1s}(r-1+\vartheta) + a_1 \tanh(z_{1s}(r-1+\vartheta)) + a_2 \tanh(z_{2s}(r-1+\vartheta)) \\
\qquad\qquad +a_3 \tanh(z_{3s}(r-1+\vartheta)) + C_1(r-1+\vartheta), \\
{}^{c}\Delta_{d}^{\vartheta} z_{2s}(r) = -z_{2s}(r-1+\vartheta) + b_1 \tanh(z_{1s}(r-1+\vartheta)) + b_2 \tanh(z_{2s}(r-1+\vartheta)) \\
\qquad\qquad +b_3 \tanh(z_{3s}(r-1+\vartheta)) + \alpha z_{2s}(r-1+\vartheta)\left(e + \beta(z_{4s}(r-1+\vartheta))^4\right) \\
\qquad\qquad +C_2(r-1+\vartheta), \\
{}^{c}\Delta_{d}^{\vartheta} z_{3s}(r) = -z_{3s}(r-1+\vartheta) + c_1 \tanh(z_{1s}(r-1+\vartheta)) + c_2 \tanh(z_{2s}(r-1+\vartheta)) \\
\qquad\qquad +c_3 \tanh(z_{3s}(r-1+\vartheta)) + C_3(r-1+\vartheta), \\
{}^{c}\Delta_{d}^{\vartheta} z_{4s}(r) = d_1 z_{2s}(r-1+\vartheta) + d_2 z_{4s}(r-1+\vartheta) + C_4(r-1+\vartheta),
\end{cases} \tag{31}
$$

where the functions C_1, C_2, C_3 and C_4 are the synchronization controllers. The synchronization error is defined for $r \in \mathbb{N}_{d-1+\vartheta}$ as follows:

$$
\begin{cases}
e_1(r) = z_{1s}(r) - z_{1m}(r), \\
e_2(r) = z_{2s}(r) - z_{2m}(r), \\
e_3(r) = z_{3s}(r) - z_{3m}(r), \\
e_4(r) = z_{4s}(r) - z_{4m}(r),
\end{cases} \tag{32}
$$

then, the master system (30) and the slave system (31) are said to be synchronized if

$$
\lim_{r \to \infty} |e_j(r)| = 0, \quad \textit{for } j = 1, 2, 3, 4. \tag{33}
$$

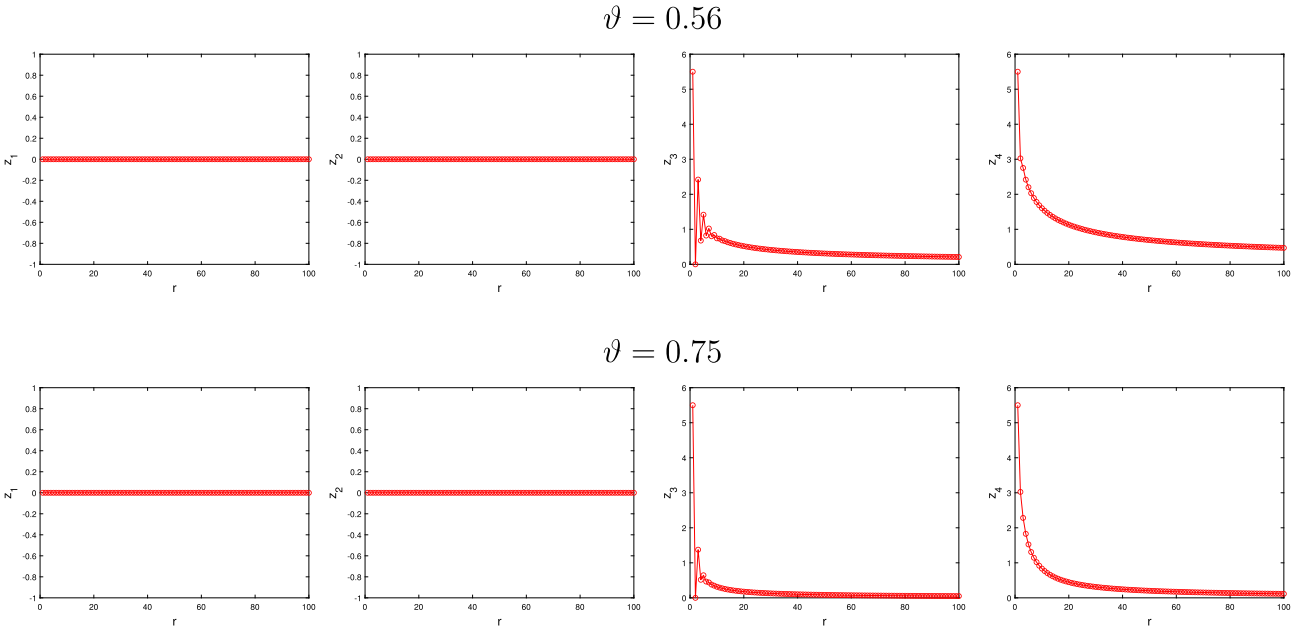

Fig. 18 The stabilized states of the controlled FDNN model(28) for $a_1 = 1.5, a_2 = 2, a_3 = 0.9, b_1 = -1.5, b_2 = 1.5, b_3 = -0.45, c_1 = 3, c_2 = -2, c_3 = 1.5, d_1 = 0.1, d_2 = -0.45, \alpha = -0.5, \beta = -0.12, e = 1.519$ and I.C.$(0, 0, 5.5, 5.5)$.

The following Theorem describes the suggested control law for attaining the synchronization of the conceived system.

Theorem 2. Subject to

$$\begin{cases} C_1(r) = -a_1(\tanh(z_{1s}(r) - \tanh(z_{1m}(r))) - a_2(\tanh(z_{2s}(r) - \tanh(z_{2m}(r))) \\ \quad -a_3(\tanh(z_{3s}(r) - \tanh(z_{3m}(r))) - l_1 e_1(r), \\ C_2(r) = -b_1(\tanh(z_{1s}(r) - \tanh(z_{1m}(r))) - b_2(\tanh(z_{2s}(r) - \tanh(z_{2m}(r))) \\ \quad -b_3\tanh(z_{3s}(r) - \tanh(z_{3m}(r))) - \alpha z_{2s}(r)\Big(e + \beta\Big((z_{4s}(r))^4\Big)\Big) \\ \quad +\alpha z_{2m}(r)\Big(e + \beta\Big((z_{4m}(r))^4\Big) - l_2 e_2(r), \\ C_3(r) = -c_1(\tanh(z_{1s}(r) - \tanh(z_{1m}(r))) - c_2(\tanh(z_{2s}(r) - \tanh(z_{2m}(r))) \\ \quad -c_3(\tanh(z_{3s}(r) - \tanh(z_{3m}(r))) - l_3 e_3(r), C_4(r) = -d_1 e_2(r) - l_4 e_4(r). \end{cases} \tag{34}$$

where $-1 < l_j < 2^{\vartheta} - 1, j = 1, 2, 3$ and $0 < l_4 - d_2 < 2^{\vartheta}$. Then the master system (30) and slave system (31) are synchronized.

Proof. By using the Caputo-type ϑ-th fractional-order differences On the error system (32), we get:

$$\begin{cases} {}^{c}\Delta_d^{\vartheta} e_1(r) = -z_{1s}(r-1+\vartheta) + a_1\tanh(z_{1s}(r-1+\vartheta)) + a_2\tanh(z_{2s}(r-1+\vartheta)) \\ \quad +a_3\tanh(z_{3s}(r-1+\vartheta)) + C_1(r-1+\vartheta) + z_{1m}(r-1+\vartheta) \\ \quad -a_1\tanh(z_{1m}(r-1+\vartheta)) - a_2\tanh(z_{2m}(r-1+\vartheta)) \\ \quad -a_3\tanh(z_{3m}(r-1+\vartheta)), \\ {}^{c}\Delta_d^{\vartheta} e_2(r) = -z_{2s}(r-1+\vartheta) + b_1\tanh(z_{1s}(r-1+\vartheta)) + b_2\tanh(z_{2s}(r-1+\vartheta)) \\ \quad +b_3\tanh(z_{3s}(r-1+\vartheta)) + \alpha z_{2s}(r-1+\vartheta)\Big(e + \beta(z_{4s}(r-1+\vartheta))^4\Big) \\ \quad +C_2(r-1+\vartheta) + z_{2m}(r-1+\vartheta) - b_1\tanh(z_{1m}(r-1+\vartheta)) \\ \quad -b_2\tanh(z_{2m}(r-1+\vartheta)) - b_3\tanh(z_{3m}(r-1+\vartheta)) \\ \quad -\alpha z_{2m}(r-1+\vartheta)\Big(e + \beta(z_{4m}(r-1+\vartheta))^4\Big), \\ {}^{c}\Delta_d^{\vartheta} e_3(r) = -z_{3s}(r-1+\vartheta) + c_1\tanh(z_{1s}(r-1+\vartheta)) + c_2\tanh(z_{2s}(r-1+\vartheta)) \\ \quad +c_3\tanh(z_{3s}(r-1+\vartheta)) + C_3(r-1+\vartheta) + z_{3m}(r-1+\vartheta) \\ \quad -c_1\tanh(z_{1m}(r-1+\vartheta)) - c_2\tanh(z_{2m}(r-1+\vartheta)) \\ \quad -c_3\tanh(z_{3m}(r-1+\vartheta)), \\ {}^{c}\Delta_d^{\vartheta} e_4(r) = d_1 z_{2s}(r-1+\vartheta) + d_2 z_{4s}(r-1+\vartheta) + C_4(r-1+\vartheta) \\ \quad -d_1 z_{2m}(r-1+\vartheta) - d_2 z_{4m}(r-1+\vartheta). \end{cases} \tag{35}$$

Substituting the control law (34) into (35), we get:

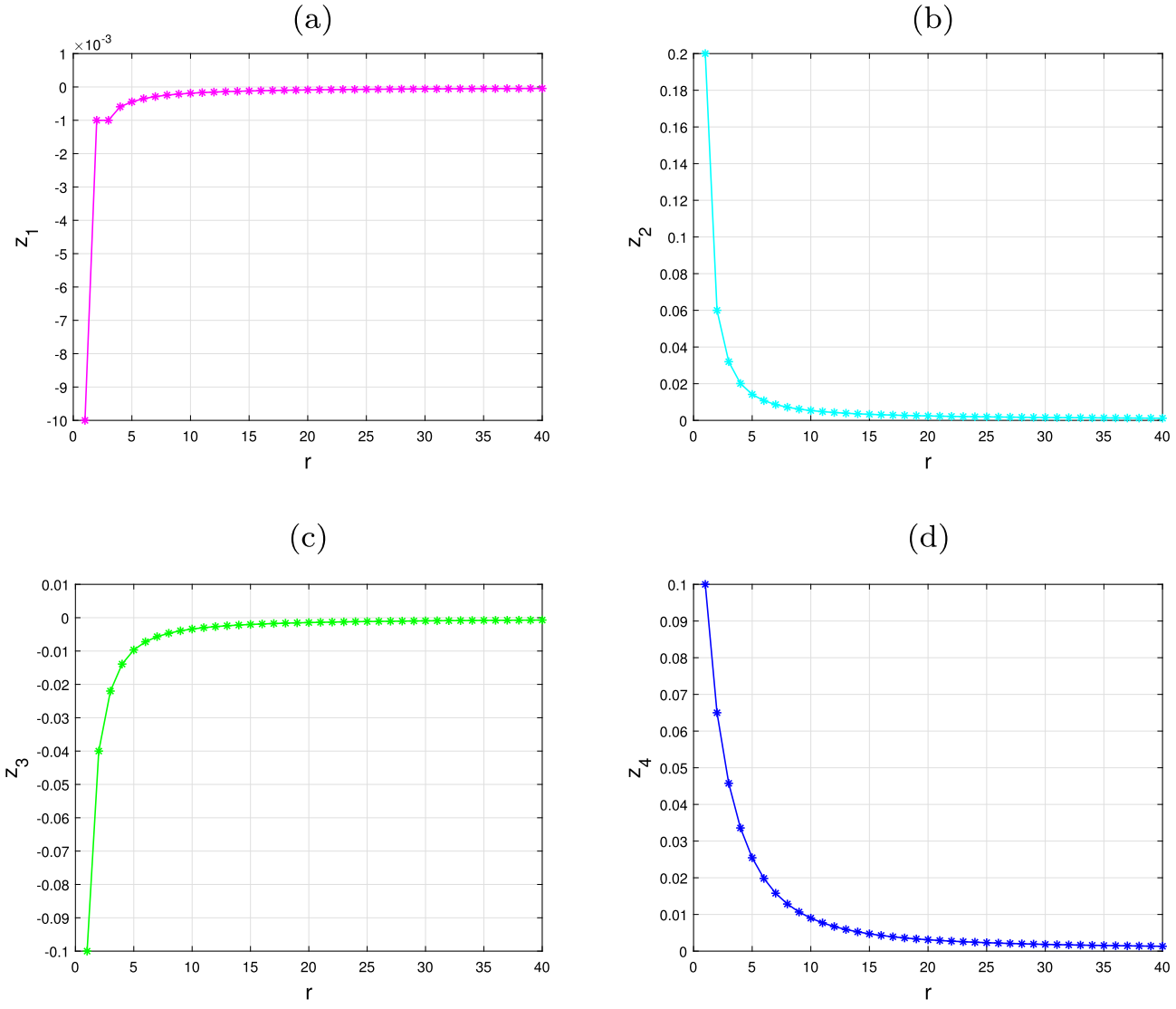

Fig. 19 Time evolution of the fractional error system (35).

$$
\begin{aligned}
&{}^{c}\Delta^{v}(e_1(r), e_2(r), e_3(r), e_4(r))^{T} \\
&\quad = B \times (e_1(r-1+\vartheta), e_2(r-1+\vartheta), \\
&\quad\ e_3(r-1+\vartheta), e_1(r-1+\vartheta))^{T},
\end{aligned} \tag{36}
$$

where

$$
B = \begin{pmatrix} -(1+l_1) & 0 & 0 & 0 \\ 0 & -(1+l_2) & 0 & 0 \\ 0 & 0 & -(1+l_3) & 0 \\ 0 & 0 & 0 & -(l_4-d_2) \end{pmatrix}
$$

The eigenvalues of the matrix B are $\lambda_1 = -(1+l_1), \lambda_2 = -(1+l_2), \lambda_3 = -(1+l_3)$ and $\lambda_4 = -(l_4 - d_2)$. Now, it is easy to see that, for $-1 < l_j < 2^{\vartheta} - 1$ where $j = 1, 2, 3$ and for $0 < l_4 - d_2 < 2^{\vartheta}$, the eigenvalues λ_i for $i = 1, 2, 3, 4$ satisfy

$$
|\lambda_i| < \left(2\cos\frac{|\arg\lambda_i| - \pi}{2 - v}\right)^{\vartheta} = 2^{\vartheta} \quad \text{and} \quad |\arg\lambda_i| = \pi > \frac{\vartheta\,\pi}{2}.
$$

So, we can conclude that according to Lemma 2, the fractional error system (35) is stabilized at zero and consequently, the fractional discrete neural network master system (30) and the fractional discrete neural network slave system (31) are synchronized.

In order to verify this result, numerical simulations are performed using MATLAB. We choose $\vartheta = 0.9, a_1 = 1.5, a_2 = 2, a_3 = 0.9, b_1 = -1.5, b_2 = 1.5, b_3 = -0.45, c_1 = 3, c_2 = -2, c_3 = 1.5, d_1 = 0.1, d_2 = -0.45, \alpha = -0.5, \beta = -0.12, e = 1.519, (l_1, l_2, l_3, l_4) = (-0.1, -0.3, -0.4, -0.1)$ and the initial values $(e_1(0), e_2(0), e_3(0), e_4(0)) = (-0.01, 0.2, -0.1, 0.1)$. Fig. 19 reports the time evolution of states of the fractional error system (35) subject to control law (34). It is evident that the errors approach zero, which provides that the synchronization discussed earlier is effective.

6. Conclusion

In this article, we described a new four-dimensional fractional discrete neural network with electromagnetic radiation model depending on commensurate, incommensurate and variable orders. The model revealed that there are different and rich dynamical characteristics. The behaviors of the suggested FDNN model for three cases: the commensurate order case, the incommensurate order case and the variable order case were discussed by calculating the Lyapunov exponent, plotting phase portraits and bifurcation diagrams and using the 0–1 test method. We have shown that the states of the proposed model are affected by the changes in values of the fractional order and the system parameters, and a variety of dynamics have been obtained, including stable trajectories, periodic motions, and chaotic behaviors. Furthermore, the ApEn algorithm and C_0 test were applied to measure the complexity of the proposed model. The results show that when the fractional orders are varied, the fractional discrete neural network model produces chaotic behavior with a higher complexity degree and a broader range of chaotic regions. Finally, successful control laws were suggested that enable stabilizing and synchronizing the suggested model by compelling the states to converge toward zero asymptotically. Numerical simulations using MATLAB were accomplished to validate our results. Owing to its complex and diverse dynamical behavior, this study can provide a theoretical framework and aid future work in the fields of secure communication and encryption.

Declaration of Competing Interest

The authors declare that they have no known competing financial interests or personal relationships that could have appeared to influence the work reported in this paper.

References

[1] J. Cao, Y. Wan, Matrix measure strategies for stability and synchronization of inertial BAM neural network with time delays, Neural Networks 53 (2014) 165–172, https://doi.org/10.1016/j.neunet.2014.02.003.

[2] D. Tank, J. Hopfield, Simple 'neural' optimization networks: An A/D converter, signal decision circuit, and a linear programming circuit, IEEE Trans. Circ. Syst. 33 (1986) 533–541, https://doi.org/10.1109/tcs.1986.1085953.

[3] S. Wen, Z. Zeng, T. Huang, Q. Meng, W. Yao, Lag synchronization of switched neural networks via neural activation function and applications in image encryption, IEEE Trans. Neural Networks Learn. Syst. 26 (2015) 1493–1502, https://doi.org/10.1109/tnnls.2014.2387355.

[4] X. Wan, X. Yang, R. Tang, Z. Cheng, H.M. Fardoun, F.E. Alsaadi, Exponential synchronization of semi-markovian coupled neural networks with mixed delays via tracker information and quantized output controller, Neural Networks. 118 (2019) 321–331, https://doi.org/10.1016/j.neunet.2019.07.004.

[5] J. Yang, L. Wang, Y. Wang, T. Guo, A novel Memristive Hopfield neural network with application in associative memory, Neurocomputing. 227 (2017) 142–148, https://doi.org/10.1016/j.neucom.2016.07.065.

[6] X. Hu, B. Jiang, J. Chen, C. Liu, Synchronization behavior in a memristive synapse-connected neuronal network, Eur. Phys. J. Plus 137 (2022) 895, https://doi.org/10.1140/epjp/s13360-022-03094-8.

[7] B. Yan, F. Parastesh, S. He, K. Rajagopal, S. Jafari, M. Perc, Interlayer and intralayer synchronization in multiplex fractional-order neuronal networks, Fractals. 30 (10) (2022) 2240194–2240592, https://doi.org/10.1142/S0218348X22401946.

[8] F. Parastesh, K. Rajagopal, S. Jafari, M. Perc, E. Schöll, Blinking coupling enhances network synchronization, Phys. Rev. E 105 (5) (2022) 054304, https://doi.org/10.1103/PhysRevE.105.054304.

[9] G.K. Sar, S.N. Chowdhury, M. Perc, D. Ghosh, Swarmalators under competitive time-varying phase interactions, New J. Phys. 24 (4) (2022) 043004, https://doi.org/10.1088/1367-2630/ac5da2.

[10] F.M. Atici, P. Eloe, Discrete fractional calculus with the Nabla operator, Electronic Journal of Qualitative Theory of Differential Eqs. (2009) 1–12, https://doi.org/10.14232/ejqtde.2009.4.3.

[11] G.A. Anastassiou, Principles of delta fractional calculus on time scales and inequalities, Mathematical and Computer Modelling. 52 (2010) 556–566, https://doi.org/10.1016/j.mcm.2010.03.055.

[12] T. Abdeljawad, On Riemann and Caputo fractional differences, Computers & Mathematics with Applications. 62 (2011) 1602–1611, https://doi.org/10.1016/j.camwa.2011.03.036.

[13] G.C. Wu, T.T. Song, S.Q. Wang, Caputo-Hadamard fractional differential equation on time scales: Numerical scheme, asymptotic stability, and chaos, Chaos 32 (2022) 093143, https://doi.org/10.1063/5.0098375.

[14] S. Majhi, M. Perc, D. Ghosh, Dynamics on higher-order networks: A review. J.R. Soc, Interface. 19 (188) (2022) 20220043, https://doi.org/10.1098/rsif.2022.0043.
[15] D. Baleanu, A. Jajarmi, H. Mohammadi, S. Rezapour, A new study on the mathematical modelling of human liver with Caputo-Fabrizio fractional derivative, Chaos, Solitons & Fractals. 134 (2020) 109705, https://doi.org/10.1016/j.chaos.2020.109705.
[16] A. Jajarmi, D. Baleanu, S.S. Sajjadi, J.J. Nieto, Analysis and some applications of a regularized Ψ–Hilfer fractional derivative, Journal of Computational and Applied Mathematics. 415 (2022) 114476, https://doi.org/10.1016/j.cam.2022.114476.
[17] O. Defterli, D. Baleanu, A. Jajarmi, S.S. Sajjadi, N. Alshaikh, J. H. Asad, Fractional treatment: an accelerated mass-spring system, Romanian Reports in Physics 74 (2022) 122.
[18] G.-C. Wu, D. Baleanu, Discrete fractional logistic map and its Chaos, Nonlinear Dynamics. 75 (2014) 283–287, https://doi.org/10.1007/s11071-013-1065-7.
[19] Z.-Y. He, A. Abbes, H. Jahanshahi, N.D. Alotaibi, Y. Wang, Fractional-order discrete-time sir epidemic model with vaccination: Chaos and complexity, Mathematics. 10 (2022) 165, https://doi.org/10.3390/math10020165.
[20] M.T. Shatnawi, A. Abbes, A. Ouannas, I.M. Batiha, A new two-dimensional fractional discrete rational map: Chaos and complexity, Physica Scripta. 98 (2022) 015208, https://doi.org/10.1088/1402-4896/aca531.
[21] D. Vignesh, S. Banerjee, Dynamical analysis of a fractional discrete-time vocal system, Nonlinear Dynamics. (2022), https://doi.org/10.1007/s11071-022-08086-y.
[22] M.T. Shatnawi, A. Abbes, A. Ouannas, I. Batiha, Hidden multistability of fractional discrete non-equilibrium point memristor based map, Physica Scripta. (2023), https://doi.org/10.1088/1402-4896/acafac.
[23] A. Abbes, A. Ouannas, N. Shawagfeh, H. Jahanshahi, The fractional-order discrete COVID-19 pandemic model: Stability and chaos, Nonlinear Dynamics. 111 (2022) 965–983, https://doi.org/10.1007/s11071-022-07766-z.
[24] A. Abbes, A. Ouannas, N. Shawagfeh, G. Grassi, The effect of the Caputo fractional difference operator on a new discrete COVID-19 model, Results in Physics. 39 (2022) 105797, https://doi.org/10.1016/j.rinp.2022.105797.
[25] A.-A. Khennaoui, A. Ouannas, S. Bendoukha, G. Grassi, R.P. Lozi, V.-T. Pham, On fractional–order discrete–time systems: Chaos, Stabilization and synchronization, Chaos, Solitons & Fractals. 119 (2019) 150–162, https://doi.org/10.1016/j.chaos.2018.12.019.
[26] A. Ouannas, A.A. Khennaoui, S. Momani, G. Grassi, V.-T. Pham, Chaos and control of a three-dimensional fractional order discrete-time system with no equilibrium and its synchronization, AIP Advances. 10 (2020) 045310, https://doi.org/10.1063/5.0004884.
[27] A. Ouannas, A.-A. Khennaoui, I.M. Batiha, V.-T. Pham, Synchronization between fractional chaotic maps with different dimensions, Fractional-Order Design. (2022) 89–121. doi:10.1016/b978-0-32-390090-4.00009-3.
[28] J. Cao, Y. Wan, Matrix measure strategies for stability and synchronization of inertial BAM neural network with time delays, Neural Networks. 53 (2014) 165–172.
[29] D. Tank, J. Hopfield, Simple neural optimization networks: An A/D converter, signal decision circuit, and a linear programming circuit, IEEE Transactions on Circuits and Systems. 33 (5) (1986) 533–541.
[30] S. Wen, Z. Zeng, T. Huang, Q. Meng, W. Yao, Lag Synchronization of Switched Neural Networks via Neural Activation Function and Applications in Image Encryption, IEEE Transactions on Neural Networks and Learning Systems. 26 (2015) 1493–1502.
[31] X. Wan, X. Yang, R. Tang, Z. Cheng, H. Fardoun, F. Alsaadi, Exponential synchronization of semi-Markovian coupled neural networks with mixed delays via tracker information and quantized output controller, Neural Networks. 118 (2019) 321–331.
[32] J. Yang, L. Wang, Y. Wang, T. Guo, A novel memristive Hopfield neural network with application in associative memory, Neurocomputing. 227 (2017) 142–148.
[33] G. Wu, T. Abdeljawad, J. Liu, D. Baleanu, K. Wu, Mittag-Leffler stability analysis of fractional discrete-time neural networks via fixed point technique, Nonlinear Analysis: Modelling and Control. 24 (2019), https://doi.org/10.15388/NA.2019.6.5.
[34] L. Huang, J. Park, G. Wu, Z. Mo, Variable-order fractional discrete-time recurrent neural networks, Journal of Computational and Applied Mathematics. 370 (2020) 112633, https://doi.org/10.1016/j.cam.2019.112633.
[35] S. Mohamad, K. Gopalsamy, Exponential stability of continuous-time and discrete-time cellular neural networks with delays, Applied Mathematics and Computation. 135 (2003) 17–38, https://doi.org/10.1016/S0096-3003(01)00299-5.
[36] L.P. Chen, H. Yin, L.G. Yuan, A.M. Lopes, J.T. Machado, R. C. Wu, A novel color image encryption algorithm based on a fractional-order discrete chaotic neural network and DNA sequence operations, Front. Inf. Technol. Electron. Eng. 21 (6) (2020) 866–879, https://doi.org/10.1631/FITEE.1900709.
[37] A. Hioual, A. Ouannas, T.-E. Oussaeif, G. Grassi, I.M. Batiha, S. Momani, On variable-order fractional discrete neural networks: Solvability and stability, Fractal and Fractional. 6 (2022) 119, https://doi.org/10.3390/fractalfract6020119.
[38] I.M. Batiha, A. Ouannas, J. Emwas, A stabilization approach for a novel chaotic fractional-order discrete neural network, Journal of Mathematical and Computational Science. 11 (2021) 5514–5524, https://doi.org/10.28919/jmcs/6004.
[39] A. Hioual, T.-E. Oussaeif, A. Ouannas, G. Grassi, I.M. Batiha, S. Momani, New results for the stability of fractional-order discrete-time Neural Networks, Alexandria Eng. J.. 61 (2022) 10359–10369, https://doi.org/10.1016/j.aej.2022.03.062.
[40] L. Chen, H. Yin, T. Huang, L. Yuan, S. Zheng, L. Yin, Chaos in fractional-order discrete neural networks with application to Image Encryption, Neural Networks. 125 (2020) 174–184, https://doi.org/10.1016/j.neunet.2020.02.008.
[41] A. Abbes, A. Ouannas, N. Shawagfeh, A.A. Khennaoui, Incommensurate fractional discrete neural network: Chaos and complexity, The European Physical Journal Plus. 137 (2022), https://doi.org/10.1140/epjp/s13360-022-02472-6.
[42] A.O. Almatroud, Extreme multistability of a fractional-order discrete-time neural network, Fractal and Fractional. 5 (2021) 202, https://doi.org/10.3390/fractalfract5040202.
[43] L.L. Huang, J.H. Park, G.C. Wu, Z.W. Mo, Variable-order fractional discrete-time recurrent neural networks, J. Comput. Appl. Math. 370 (2020) 112633, https://doi.org/10.1016/j.cam.2019.112633.
[44] A. Hioual, A. Ouannas, T.-E. Oussaeif, G. Grassi, I.M. Batiha, S. Momani, On variable-order fractional discrete neural networks: Solvability and stability, Fractal and Fractional. 6 (2022) 119, https://doi.org/10.3390/fractalfract6020119.
[45] R.C. Karoun, A. Ouannas, M.A. Horani, G. Grassi, The effect of Caputo fractional variable difference operator on a discrete-time Hopfield neural network with non-commensurate order, Fractal and Fractional. 6 (2022) 575, https://doi.org/10.3390/fractalfract6100575.
[46] A. Hioual, A. Ouannas, G. Grassi, T.-E. Oussaeif, Nonlinear nabla variable-order fractional discrete systems: Asymptotic stability and application to Neural Networks, Journal of Computational and Applied Mathematics. 423 (2023) 114939, https://doi.org/10.1016/j.cam.2022.114939.

[47] F.M. Allehiany, E.E. Mahmoud, L.S. Jahanzaib, P. Trikha, H. Alotaibi, Chaos control and analysis of fractional order neural network under electromagnetic radiation, Results in Physics. 21 (2021) 103786, https://doi.org/10.1016/j.rinp.2020.103786.

[48] G.-C. Wu, D. Baleanu, Jacobian matrix algorithm for Lyapunov exponents of the discrete fractional maps, Commun. Nonlinear Sci. Numer. Simul. 22 (2015) 95–100, https://doi.org/10.1016/j.cnsns.2014.06.042.

[49] G.A. Gottwald, I. Melbourne, The 0–1 test for chaos: A Review, Chaos Detection and Predictability. (2016) 221–247. doi:10.1007/978-3-662-48410-4_7.

[50] S.M. Pincus, Approximate entropy as a measure of system complexity., Proceedings of the National Academy of Sciences. 88 (1991) 2297–2301. doi:10.1073/pnas.88.6.2297.

[51] S. En-hua, C. Zhi-jie, G. Fan-ji, Mathematical Foundation of a new complexity measure, Appl. Math. Mech. 26 (2005) 1188–1196, https://doi.org/10.1007/bf02507729.

[52] S. He, K. Sun, H. Wang, Complexity analysis and DSP implementation of the fractional-order Lorenz hyperchaotic system, Entropy. 17 (2015) 8299–8311, https://doi.org/10.3390/e17127882.

[53] J. Čermák, I. Győri, L. Nechvátal, On explicit stability conditions for a linear fractional difference system, Fractional Calculus and Applied, Analysis. 18 (2015) 651–672, https://doi.org/10.1515/fca-2015-0040.